Title: Anticipatory responses along motion trajectories in awake monkey area V1

Authors

Giacomo Benvenuti[1‡], Sandrine Chemla[1], Arjan Boonman[1†], Laurent Perrinet[1], Guillaume S Masson[1], Frédéric Chavane[1]*

Affiliations

[1]Institut de Neurosciences de la Timone (INT), CNRS and Aix-Marseille Université, UMR 7289, Campus Santé Timone, 27 boulevard Jean Moulin, Marseille 13005, France.

‡ Current address: Center for Perceptual Systems, University of Texas, Austin, Texas 78712, USA

†Current address: Department of Zoology, Faculty of Life Sciences, Tel Aviv University, Tel Aviv 6997801, Israel

*Correspondence: frederic.chavane@univ-amu.fr

Highlights

- Our hypothesis is that lateral propagation of activity in V1 contributes to the integration of translating stimuli

- Consistent with this hypothesis, we find that a translating bar induces anticipatory spiking activity in V1 neurons.

- A V1 model describes how this anticipation can arise from inter and intra-cortical lateral propagation of activity.

- The dynamic of VSDi and LFP signals in V1 is consistent with the predictions made by the model.

- The intra-cortical origin is further confirmed by the fact that a bar moving from the ipsilateral hemifield does not evoke anticipation.

- Horizontal and feedback input are not only modulatory but can also drive spiking responses in specific contexts.

ABSTRACT

What are the neural mechanisms underlying motion integration of translating objects? Visual motion integration is generally conceived of as a feedforward, hierarchical, information processing. However, feedforward models fail to account for many contextual effects revealed using natural moving stimuli. In particular, a translating object evokes a sequence of transient feedforward responses in the primary visual cortex but also propagations of activity through horizontal and feedback pathways. We investigated how these pathways shape the representation of a translating bar in monkey V1. We show that, for long trajectories, spiking activity builds-up hundreds of milliseconds before the bar enters the neurons' receptive fields. Using VSDI and LFP recordings guided by a phenomenological model of propagation dynamics, we demonstrate that this anticipatory response arises from the interplay between horizontal and feedback networks driving V1 neurons well ahead of their feedforward inputs. This mechanism could subtend several perceptual contextual effects observed with translating objects.

INTRODUCTION

In standard information processing models of the visual system, low-level visual features are extracted locally within selective receptive fields and are rapidly relayed to downstream areas in order to encode increasingly complex features (Fukushima, 1980; Riesenhuber and Poggio, 1999). When probed with spatially stationary stimuli centered on their receptive fields, properties of visual neurons from V1 to extra-striate areas are indeed well captured by a simple cascade of *linear-nonlinear models* encoding low-level visual properties such as local orientation or motion direction (Carandini et al., 2005; Rust et al., 2006) as well as more complex visual pattern (David et al., 2006; DiCarlo et al., 2012). A well-known example is given by *visual motion integration* where three decades of studies have been conducted almost exclusively with motion signals presented within a stationary aperture, such as drifting periodic stimuli or random dot patterns, centered on neuronal receptive fields (**RF**). The reported neuronal properties have provided strong evidences for the *linear-nonlinear cascade* theoretical framework, where V1 neurons encode local ambiguous motion signals that are integrated by MT neurons to compute direction and speed of pattern motion (Movshon et al., 1985; Rust et al., 2006; Simoncelli and Heeger, 1998; Wilson et al., 1992).

However, natural objects often move along extended and smooth spatio-temporal trajectories within the visual field. A handful of psychophysical, computational and physiological studies (Watamaniuk & Mc Kee 1995, Watamaniuk et al 1995, Burgi et al., 2000; Perrinet and Masson, 2012; Tlapale et al., 2010) have proposed that the visual system can use the spatio-temporal regularity of smooth trajectories to solve many of the uncertainties inherent to visual motion such as aperture (Marr, 1982; Wallach, 1935) and correspondence problems (Ullman, 1979; Wertheimer, 1912) and to improve the *signal to noise ratio* of visual input evoked by moving stimuli (e.g. Burgi et al., 2000). This idea is consistent with the view that visual systems can

80 benefit from contextual information and internal models of the statistics of the visual world
81 (Berkes et al., 2011; Geisler, 2008).

82 For example, the property of smoothness associated to motion trajectories can be used by the
83 visual system to generate internal models of moving objects (i.e. priors). In accordance with this
84 hypothesis, there is a rich psychophysical literature demonstrating how spatio-temporal
85 coherence affects the way we perceive moving stimuli attributes such as (1) position (MacKay,
86 1958; Nijhawan, 1994; W. Metzger, 1932), (2) direction (Anstis and Ramachandran, 1987;
87 Lorenceau et al., 1993; Ramachandran and Anstis, 1983; Welch et al., 1997), (3) motion (Van
88 Doorn and Koenderink, 1984; Nakayama and Silverman, 1984; Neri, 2014; Snowden and
89 Braddick, 1989b; Verghese and Watamaniuk, 1999; Verghese et al., 2000; Watamaniuk and
90 McKee, 1995; Watamaniuk et al., 1995), (4) speed (Castet et al., 1993; Georges et al., 2002;
91 McKee and Welch, 1985; Scott-Brown and Heeley, 2001) (5) orientation (Alais and Lorenceau,
92 2002; Fredericksen et al., 1994; Guo et al., 2004; Pavan et al., 2011; Werkhoven et al., 1990) and
93 (6) color (Watanabe and Nishida, 2007). For example, a target stimulus presented at the leading
94 edge of a smooth trajectory has been shown to be easier to detect than when presented in
95 isolation or at the trailing edge of the trajectory (Arnold et al., 2014; Lenkic and Enns, 2013; Liu
96 et al., 2006; Roach et al., 2011; Schwiedrzik et al., 2007). This phenomenon cannot be simply
97 explained by a shift in spatial attention, lateral facilitation or retinal motion and it is more likely
98 implemented at an early stage of visual processing (Roach et al., 2011). Furthermore, stimuli
99 presented at the leading edge of long smooth trajectories are perceived having higher resolution
100 (i.e. lower blurring due to motion) than stationary moving stimuli (Burr and Ross, 1986;
101 Watanabe and Nishida, 2007) and are more easily trackable behind occlusions (Watamaniuk and
102 McKee, 1995).

103

104 Several computational studies suggest that a simple hierarchical feedforward model with
105 contiguous local filters sequentially activated by the translating stimulus is insufficient to
106 account for these contextual effects. In contrast, they proposed that a *mechanism involving*
107 *lateral propagation across the sequence of filters activated along the trajectory* could explain the
108 emergence of motion trajectory effects (Burgi et al., 2000; Grzywacz et al., 1995; Kaplan et al.,
109 2013; Khoei et al., 2017; Perrinet and Masson, 2012; Tlapale et al., 2010; Yuille and Grzywacz,
110 1989). These models postulate that lateral interactions in early visual areas could participate in
111 processing the responses evoked by smooth trajectories of translating stimuli. Early visual areas
112 are "retinotopically organized" (Van Essen and Newsome, 1984; Hubel and Wiesel, 1974), such
113 that translating stimuli generate a sequential activation of contiguous locations on the retinotopic
114 map. Since neurons in these areas are tightly connected to their neighbors through horizontal
115 connections and feedback loops (Angelucci et al., 2002; Benucci et al., 2007; Bringuier et al.,
116 1999; Bullier, 2001; Chavane et al., 2011; Girard et al., 2001; Grinvald et al., 1994; Jancke et al.,
117 2004a; Muller et al., 2014; Reynaud et al., 2012; Slovin et al., 2002) see review (Muller et al.,
118 2018) (**Figure 1A**), feedforward responses at each location can rapidly spread to contiguous
119 areas of the map before the translating stimulus enters their RF (Jancke et al 2004, Chemla et al

2019). Consequently, the neural population mapping the leading edge of the translating stimulus will receive convergent lateral and FF inputs. These two signals may be recursively integrated along the motion trajectory and generate a gradual build-up of neural activity that would carry trajectory information. The advantage of such integration mechanism is that it would combine only the spatio-temporally coherent responses evoked by translating stimuli.

The aim of this study is to investigate this intriguing hypothesis. The primary visual cortex (**V1**) is a good candidate circuit to support such trajectory-based computation as it has the largest and most precise retinotopic representation of the outside world (Hubel and Wiesel, 1974; Tootell et al., 1982). To understand how V1 networks map motion trajectories, it is thus necessary to elucidate the interactions between feedforward, feedback and lateral networks at the proper spatio-temporal recording scales.

To achieve this goal, we recorded both single-unit and neuronal population activities in the primary visual cortex of four awake, fixating, monkeys to map the dynamics of the cortical responses to a translating bar. By using different trajectory lengths, we manipulated the history of cortical activation elicited by the moving bar before reaching the classical RF of the recorded neuron. Using single-unit recordings, we found that for long trajectories, about half of V1 neurons demonstrate a significant build-up of anticipatory spiking responses long before the bar enters their classical receptive field. Using a computational model, we show that the specific dynamics of spiking anticipatory responses could be explained by an intra-cortical horizontal and feedback network propagating information faster than the feedforward input sequence. Using voltage-sensitive dye imaging (**VSDi**) to measure the aggregate membrane potential of a large V1 area, we showed indeed that the neural population response to a translating bar exhibits a spatio-temporal structure consistent with the predictions of the model. To test whether feedback signals could also contribute to this anticipatory activity, we used a multi-electrode array to measure local field potential (**LFP**) responses across the V1 area and showed that a bar moving over a long trajectory elicits a strong and very early decrease of low frequency power, a signal recently attributed to feedback modulation (Bastos et al., 2014; Engel and Fries, 2010; van Kerkoerle et al., 2014). The intra-cortical origin of these anticipatory responses was further demonstrated by the observation that anticipation was abolished when the bar translation was initiated from the ipsi-lateral visual hemi-field. Altogether, these results dissect out the multiple scales at which an intricated network of connectivities within and between visual areas leads to the emergence of an anticipatory spread of activity that shall contribute to processing of translating objects.

RESULTS

The goals of this study were to test whether trajectory-dependent responses to a translating bar can be observed in V1 and, if so, understand the underlying network mechanisms.

Anticipatory spiking responses

We first recorded spiking responses from 80 V1 single-units in two alert, fixating macaques presented with three visual stimulation paradigms. Neurons were selected regardless of their tuning properties. For each neuron, we first mapped the spatial profile of the classical RF using sparse noise sequences and the orientation and direction tunings, using a translating bar (12 directions). Then, a vertical bright bar (0.5x4 degrees of visual angle, **dva**) was moved horizontally at 6.6 dva/s starting at either 1.5, 3 or 6dva (short, medium and long trajectories respectively) from the RF centre and disappearing 1.5-2dva beyond it (**Figure 1A**). Critically, these three trajectories stimulated the RF in exactly the same way. However, in the medium and long trajectory conditions, the translating bar had a different history, activating a large area outside of the RF through a smooth path before reaching it.

For each cell, the responses for the three trajectory conditions were aligned relative to the absolute position of the bar (**Figure 1B-F**). On the other hand, for comparing the evoked responses across cells (**Figure 1E-F**), we aligned all time-courses relative to the latency of the response evoked by the short path condition. This operation led to the automatic exclusion of 31 cells for which the detection of this important reference point was not possible due to low signal-to-noise ratio (see Methods) and the fact that stimulus direction and orientation were not optimized for the cells' preference.

In the remaining 49 cells, the time-course of the responses (PSTH) to the shortest (1.5dva) motion trajectory presented a typical fast transient rise and a slower decrease (**Figure 1B-F,** black trace). However, when the bar trajectory started 3dva or 6dva before the RF centre (dark and light blue curves, respectively), a ramp-like increase of the discharge-rate was observed before the response-onset for the shortest motion trajectory, in half (53%) of the neurons (**Figure 2A**). Such anticipatory build-up scaled up with the trajectory length. In the other neurons, responses were identical for the three trajectory conditions (**Figure 1D & figure supplement 1**), excluding that anticipatory responses were due to a systematic bias in our specific experimental approach (e.g. stimulation protocol, general bias due to eye movements, generalized allocation of spatial attention, generalized effect due to the input from LGN). On average, latencies for the medium (3dva) and long (6dva) trajectories started respectively 116ms (std =93ms) and 220ms (std = 189ms) before the latency to the shortest path (1.5dva), a decrease which was found significant over the whole population (two-sample t-test P<0.05, see **Figure 2D**). This timing corresponded to an average distance of 2.3 and 3dva between the bar position and the RF centre. In contrast, both time-to-peak and response offset remained similar across all trajectories (two-sample t-test P>0.05), excluding a spatial shift of the RF or an unspecific gain effect.
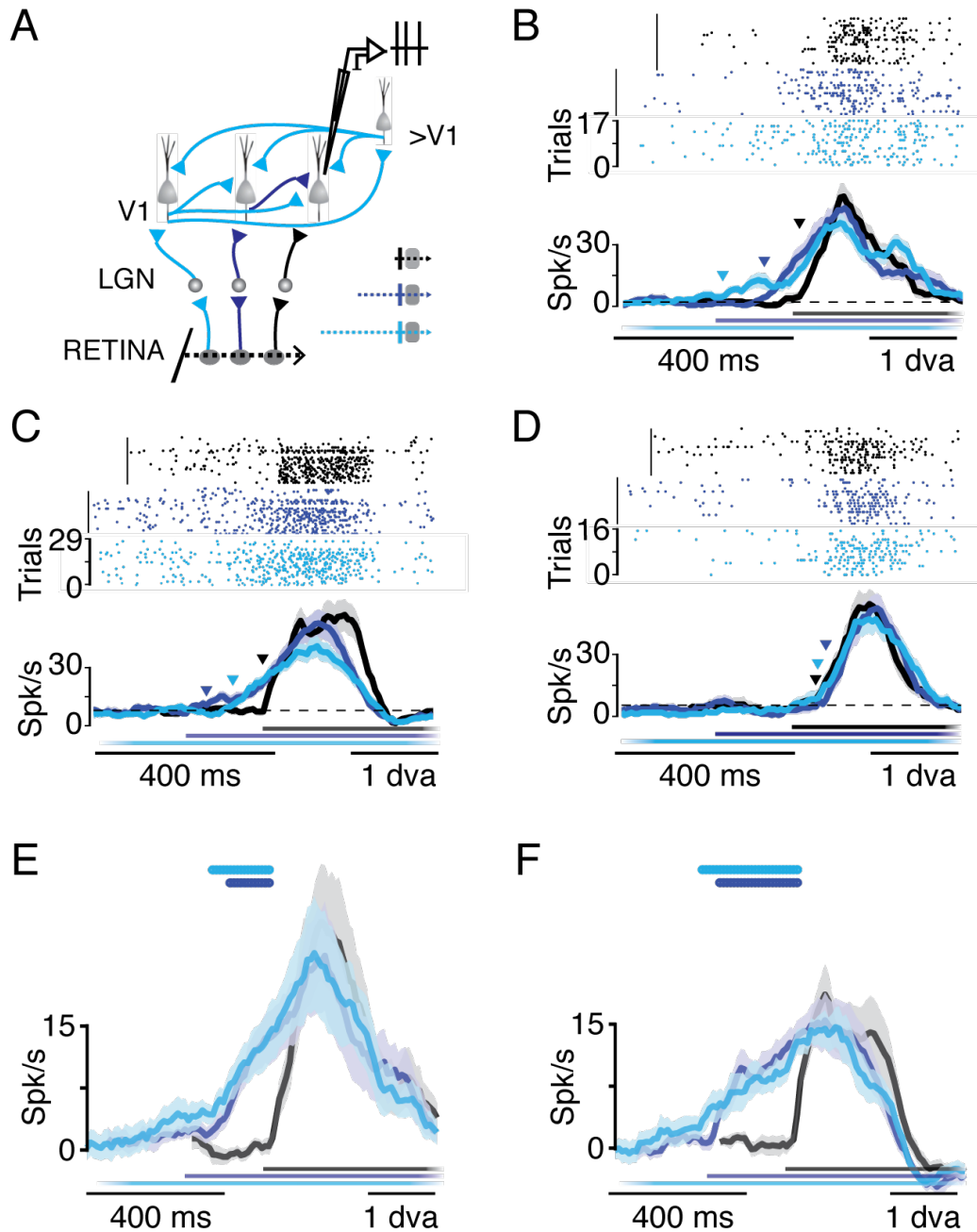
Figure 1. Single units responses to a translating bar as a function of its trajectory length outside the RF. (**A**) Experimental approach. Schematic of the retino-thalamo-cortical neural circuit. A translating bar (bottom) is going to cross consecutive V1 RFs (grey disks) eliciting a sequence of feedforward activations, propagating laterally across the retinotopic map through intra (i.e. horizontal) and inter-cortical (feedback-loops) connections. Neurons with the RF at the end of the trajectory are recorded extracellularly using an electrode (top-right). The inset on the right depicts the paths of the three trajectories (dotted lines, 1.5, 3 and 6dva, respectively) with respect to the RF (grey circle). The color-code is consistent throughout figures. (**B-D**) Examples of single unit responses for the three trajectory lengths presented with raster plots (top) and PSTHs (bottom) (B and D: Monkey PD, C: Monkey NO). B

206   and C are examples of neurons presenting anticipation, D of a neuron that does not. Colored lines
207   (bottom) indicate the stimulus presentation time, for each condition. Latency is indicated by triangles.
208   Shades represent the standard error of the mean (SEM) across trials. (**E-F**) Average PSTHs across
209   anticipatory neurons for the three trajectories, for monkeys PD (n=13) and NO (n=13), respectively.
210   Responses are aligned to the latency of the short trajectory condition. Colored lines (top) indicate
211   significant difference with respect to the short trajectory condition (two-sample t-test P<0.05).

212   This anticipatory activity extended well beyond the size of the measured RF, similar to classical
213   results (Angelucci et al., 2002), and was neither correlated with the RF sizes nor could be
214   explained by a systematic bias in monkeys' fixation (see **figure supplement 2**). The gradual rise
215   of this anticipatory response, furthermore, contrasts with the transient profile of the neural
216   response for a bar swept over the RF and suggests a slower cumulative process. These
217   anticipatory responses merged ~100ms before the short-trajectory response onset and from then
218   followed an identical dynamic. This asymmetry eliminates the possibility that the response build-
219   up would be related to a systematic misestimation of the classical RF position or size, that would
220   have resulted in a change in response peak time for instance. Next, we aimed at better
221   characterizing the origin of the cell-to-cell variability in the observed anticipatory responses, and
222   its relationship to the tuning of the cells.

223

224   **Understanding the diversity of degrees of anticipation**
225   To estimate the proportion of cells showing a significant modulation of firing rate over time, we
226   compared spike counts across trials in short (i.e. 1.5 dva) *vs* long (3 & 6 dva) trajectories
227   conditions. The proportion of cells significantly activated (Two-sample t-test P<0.05) at different
228   time bins along the motion trajectory gradually increased (**Figure 2A**), such that 53% of them
229   showed a significant anticipatory response 100ms before the bar entered the classical RF, for
230   long (3dva and/or 6dva, green) but not short (1.5dva, black) trajectories. By comparison, when
231   the bar entered the classical RF (i.e. vertical dotted line), all three conditions drove the same
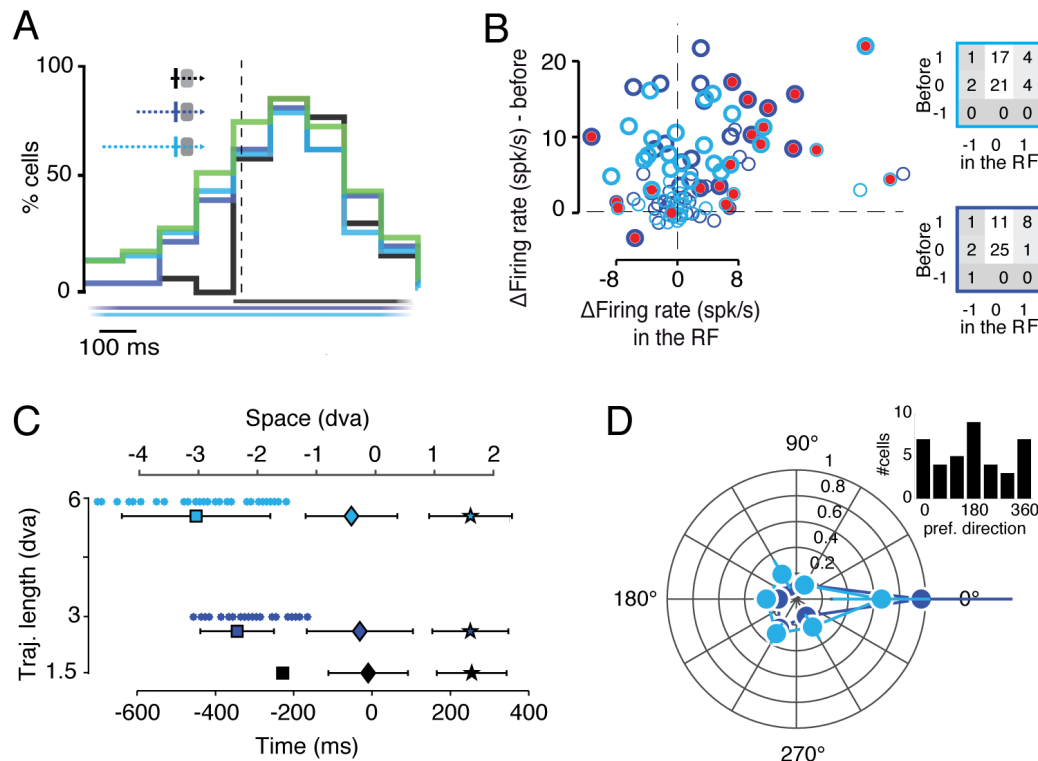232   number of cells.

233

Figure 2. Amplitudes, latencies and tunings of trajectory dependent responses. (**A**) Proportion of neurons (out of a total of n=49) showing a significant response over time for all 3 trajectory conditions (see cartoon in insert). Green color represents proportion of neurons showing a significant response only for the medium and/or long trajectory conditions. Colored lines at the bottom indicate stimulus presentation for the three trajectories. (Top-left) same inset than **Fig1A**. (**B**) Difference of firing rate between responses to long (3-6dva) and short (1.5dva) trajectory lengths before entering the RF (thick when significant) vs within the RF (red filled when significant). Before and within the RF was estimated using the latency of the short trajectory response. Table on the top: number of cells presenting a significant increase (1), decrease (-1) or no change (0) in firing-rate rate in long trajectories compared to short trajectories. Table on the bottom: same than table on the top but for medium trajectories (**C**) Mean onset latencies (square), peak response times (diamond) and offset response time (stars) for the three trajectories conditions as a function of trajectory length averaged across neurons and monkeys (n=49). Time 0 is when the bar crosses the RF center. Dots indicate latencies of individual medium and long trajectories responses. An second abscissae is drawn at the top to indicate the equivalent visual distance (dva) from the receptive field center. (**D**) Polar histogram representing the normalized averaged anticipatory response strength (computed in a time window 100ms before the latency of the short trajectory) as a function of neurons direction preference (n=32, only cells with DI>0.1). Inset: number of cells preferring each direction.

252

In a few neurons, the two longest trajectories resulted in a significantly different spiking response in the RF center (e.g. the example in **Figure 1C**). This result could provide an important evidence in support of the predictive coding theory, as prediction would result in smaller error signal and hence a smaller neuronal response (Alink et al., 2010; Mumford, 1992;

257 Srinivasan et al., 1982). However, this effect was not evidenced in the average response profiles
258 (**Figure 1E-F**) although it could have been smoothed out because of the variability in response
259 latencies. Hence, we compared individual discharge rates between short and long trajectories in
260 two different time-windows of 100ms: one placed just before (ordinate) and one just after
261 (abscissae) response latency (as estimated by detecting the first significant change with respect to
262 the baseline) for the short trajectory condition (i.e. the RF border) (**Figure 2B**). A small fraction
263 of the cells exhibiting an anticipatory build-up of activity responded slightly less when the bar
264 crossed their RF center (upper left quadrant in Figure 2B). However, such decrease was
265 significant in only 4% of the cells while, on the contrary, 16% displayed a significant increase of
266 their response in the RF (insets). These results rule out a systematic relationship between the
267 occurrence of an anticipatory build-up and a modulation of the stimulus-driven responses within
268 the RF center.

270 Next, we compared, for every neuron, the latencies for medium and long trajectories vs. the
271 latency for the short one (**Figure 2C**). This analysis revealed a continuum in the timing of
272 anticipation as shown by the latency scatter for the medium and long trajectories that fully
273 covered a wide range of values from 0 to -400 and -800ms, respectively. While the distributions
274 of response onset latencies were significantly different for the three trajectories conditions (two-
275 sample t-test $p<0.05$) both time-to-peak and response offset latencies distributions were not
276 significantly different across all trajectories (two-sample t-test $p>0.05$). We checked if the
277 variability in anticipatory responses across all neurons can be due to differences in their tuning
278 properties. Selecting neurons with a direction index > 0.1 we probed the relationship between the
279 relative firing rate in the 100ms time-window before the bar enters the RF and direction
280 preferences (**Figure 2D**). Indeed, neurons with a preferred direction aligned to the stimulus
281 motion direction exhibited a stronger anticipatory response. Therefore, the diversity of the
282 anticipation timing and strength of the response across neurons may simply reflect a direction-
283 selective anticipatory mechanism.

285 Overall, we demonstrate that a large population of V1 neurons exhibits a slow build-up of
286 activity prior a moving input hits their receptive field. Such anticipatory activity occurs sooner
287 for longer trajectories (**Figure 2C,** squares). In comparison, both the response peak and offset
288 response time did not change with trajectory length (Figure 2C, diamond and stars respectively).
289 Our next goal was to understand what neural mechanisms could generate this anticipatory
290 response.

291 **Anticipation is an expected emergent property of intra-cortical propagation**
292 These characteristics of observed anticipatory responses can be used to theoretically constrain
293 the putative underlying neural mechanisms. First, these responses emerge well before the
294 stimulus enters the classical RF of the recorded neurons. Second, the decrease in onset latency is
295 not followed by a similar shift in time-to-peak and offset latency. Eventually, anticipatory
296 responses present a slow dynamic consisting of a gradual rise of activity. A feedforward network

297   alone is unlikely to account for the slow dynamics and the asymmetry of these responses.
298   Alternatively, these features are consistent with surround modulation (Bair et al., 2003; Klink et
299   al., 2017; Nassi et al., 2013; Reynaud et al., 2012). Visual information from the RF surround can
300   be provided to V1 neurons from intra-cortical horizontal (**H**) and inter-cortical feedback (**FB**)
301   networks (Angelucci and Bressloff, 2006; Roelfsema, 2006). We therefore reasoned that the
302   anticipation we observed in V1 shall arise from the interactions between feedforward and intra-
303   cortical inputs carried by horizontal and feedback connections. To test this hypothesis, we
304   disentangled the contribution of these signals to anticipatory responses by using the well know
305   intrinsic differences in the spatial and temporal scales of these inputs. To do so, we developed a
306   simple phenomenological, but biologically-plausible, model simulating feed-forward and
307   cortico-cortical responses within a cortical retinotopic map (**Figure 3A,** see Methods and **figure**
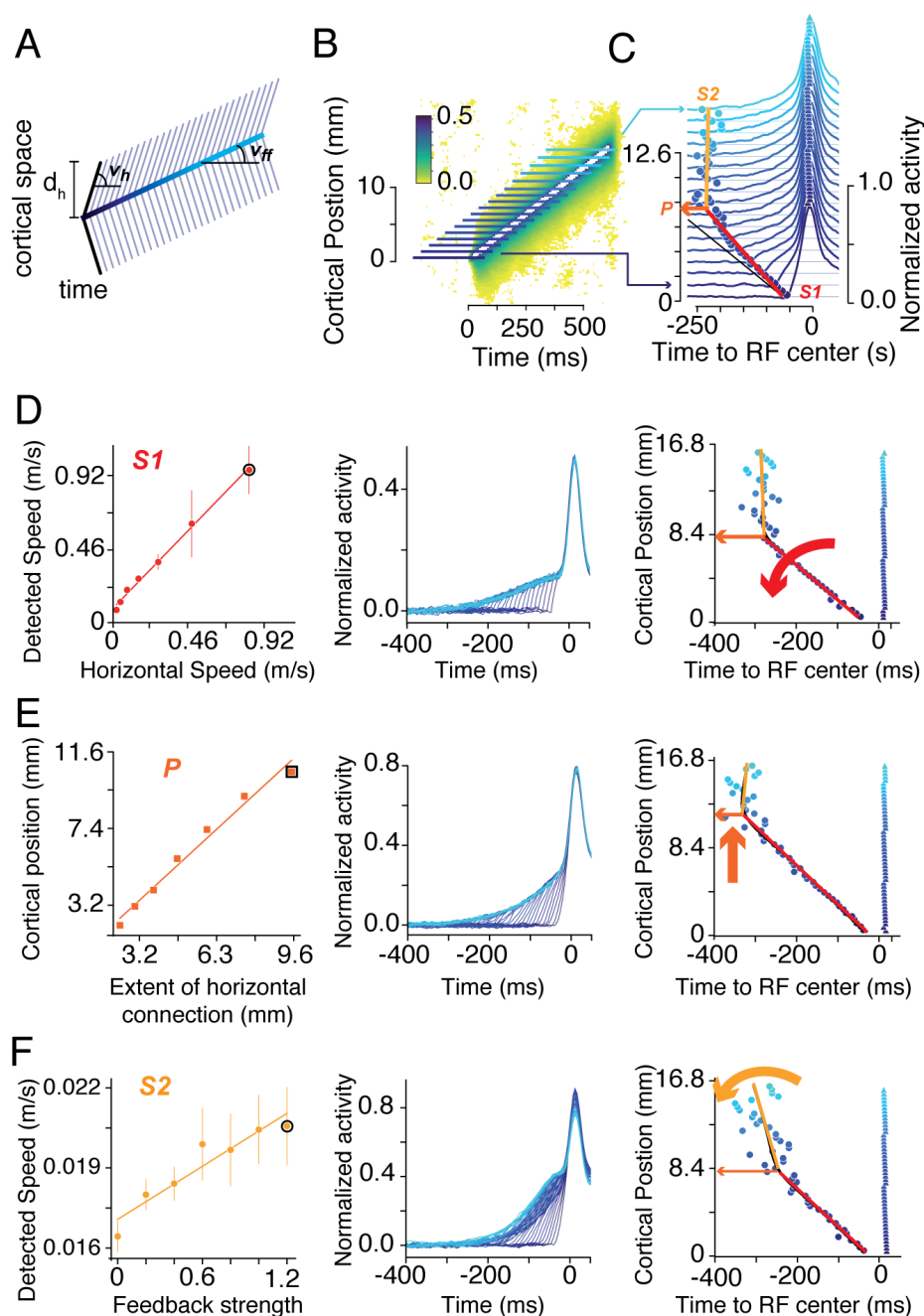308   **supplement 3**).
309
310

Figure 3. A physiologically plausible model of lateral cortical integration. (**A**) Cartoon describing the model developed to predict the time-course of the neural population response to a translating bar in the space-time domain. The translating bar evokes a sequence of spatio-temporal feedforward activation of the cortex at a speed of v_{ff} (thick blue line, blue hue codes for time). The feedforward activation is then relayed by horizontal propagation at speed v_h and over a distance of d_h represented by thinner obliques lines. (**B**). Activation of the model when v_{ff}, v_h and d_h are set to values compatible with our visual stimulation paradigm and the know horizontal network properties of the cortex (Angelucci et al., 2002; Girard et al., 2001; Grinvald et al., 1994; Muller et al., 2014). Color-code represents cortical activation strength (arbitrary units). (**C**) Time-course of the neural population response at different positions along the trajectory. Traces are aligned to the time of the feedforward arrival in the receptive field centre (the

322   stimulus onset is displayed as a slant dark line). For each response time-course, latency is indicated by a
323   disk. The profile of latency changes with the increase of the trajectory length is captured by a piecewise
324   linear regression (red and orange lines) showing a first decrease with a slope S1 up to a position P,
325   followed by a second slope S2. (**D**) Effect of changing the speed v_{ic} on the slope S1 (left). The middle and
326   right panel shows, for a speed example (black circle in the left panel), an example of time-courses and the
327   plot of latencies as a function of distance along the trajectory (with extraction of S1, P and S2). (**E**) Same
328   as in D but for changes of d_{ic}. (**F**) Same as in D but for changes of feedback strength.

330   The response to a bar translating along an extended, straight, trajectory was modelled as a
331   sequence of feedforward activations at different spatiotemporal positions, changing with speed
332   v_{ff} (**Figure 3A**). At each spatiotemporal position, this feedforward input also gave rise to an
333   isotropic horizontal propagation of activity with speed v_h over a cortical distance d_h (**Figure 3A**).
334   When $v_h > v_{ff}$, the model qualitatively predicts the emergence of a gradual anticipatory build-up
335   of activity whose onset latency depends on trajectory length (**Figure 3C**). This effect is a
336   consequence of the speed difference between the sequence of feedforward activations (i.e.
337   stimulus speed) and the horizontal propagation: after an initiation phase, a given cortical position
338   will receive information about the approaching bar first from the intra-cortical propagation (i.e.
339   anticipatory response) and second from the feedforward input. For each position, after realigning
340   the time-course of activation patterns to the end of all trajectories, we observed a gradual
341   emergence of an anticipatory activation, whose latency (blue dots) decreases with trajectory
342   length (color-coded as hue of the blue) and reaches saturation for distances larger than d_h (**Figure
343   3D**). Beyond this distance, the latencies of anticipatory responses do not change anymore simply
344   because of the absence of direct anatomical horizontal connections. In other words, to generate a
345   latency decrease, the bar needs to reach a region that is directly connected to the recording site.

347   To capture this behavior, we used a piecewise linear regression of the latency as a function of
348   trajectory length. From this regression, we extracted the slope of the change in the response
349   latency at the beginning and at the end of the trajectory (**S1** and **S2** respectively) and the position
350   of intersection between these regression lines (**P**). These 3 parameters correspond to the speed at
351   which latency of anticipatory activity decrease along the trajectory (S1), the spatial limit of this
352   decrease (P) and the rate of latency changes for distances beyond this position (S2). To
353   understand how does the spatio-temporal properties of the intra-cortical propagations affect these
354   three parameters, we varied v_h and d_h over a large range of values. As predicted, we found that
355   **S1** and **P** are under control of v_h and d_h respectively, which linearly modulate these parameters
356   over a large range of values (**Figure 3D and E**). In short, the properties of the intra-cortical
357   propagation directly influence the speed and the extent of the latency decrease.

359   This observation has two theoretical consequences. First, if anticipation would result from a
360   large divergence of the feedforward inputs, we should observe a latency decrease at a fixed delay
361   after stimulus onset since all thalamic input arrive with the same latency. As a result,
362   anticipation should not be trajectory-dependent and should generate a very high speed S1
363   (**Figure 3D**). Second, the spatial extent of the observed latency decrease should be equivalent to

364   anatomical extent of the anatomical divergence (**Figure 3E**). In the following section, we tested
365   the validity of this model with further neural recordings at different scales.
366

VSD imaging unveils an intra-cortical propagation of anticipatory activity

368   Our model produces testable predictions for the spatiotemporal profile of V1 population
369   responses to a translating stimulus. To test these predictions, we need to record cortical activity
370   at both high resolution and large field of view in order to measure the fine change of response
371   latency as a function of trajectory length. To do so, we used voltage-sensitive dye imaging
372   (**VSDi**), a mesoscopic imaging technique with high spatial and temporal resolution. Since this
373   technique reveals the aggregate membrane potential oscillations of the cortex (Grinvald and
374   Hildesheim, 2004), we can dissect out the effect of cortical propagation with a high sensitivity.
375   In a third, awake and fixating, monkey (WA), we measured population synaptic activity using
376   VSDi (**Figure 4A**) over a large cortical region representing retinotopically -2dva to 0dva of
377   azimuthal eccentricity.
378

379   The translating bar elicited a wave of VSD activity propagating across the retinotopic map at the
380   expected speed and direction of the bar motion trajectory. More important, a strong anticipatory
381   activity was also detectable at the early frames for the medium and long trajectories (**Figure 4B**).
382   Notice that, since the VSDi signal reflects the combination of both the sub and supra-threshold
383   response components (Chemla and Chavane, 2010; Chen et al., 2012), this observation at
384   population level indirectly confirms the spiking results in a third monkey but with a different
385   technique. For similar retinotopic positions, the anticipatory response evoked by the moving bar
386   was stronger for the long trajectory than the one for the medium trajectory (compare first 4
387   panels in Figure 4B) confirming the slow build-up of activity reported above. Our model
388   demonstrates how such slow dynamics can be a signature of lateral propagation of activity and
389   not a divergent feedforward network.
390

391   To facilitate the qualitative comparison with the model simulations shown in **Figure 3C**, we
392   displayed the time course of the VSDi responses as being aligned to the end of the trajectories
393   and sorted accordingly to their distance from the initial bar position (blue hue color code, **Figure**
394   **4D**, top panel). For each cortical position, the anticipatory VSD activity started growing slowly a
395   few hundreds of milliseconds before the bar reached the corresponding retinotopic positions.
396   Beyond this point, responses were identical across all conditions, similarly to what was observed
397   at the spiking level, and in close agreement with model predictions. We measured both onset
398   (vertical ticks at the bottom of Figure 4D top panel) and peak latencies for each condition and
399   plotted them as a function of the distance (in visual angle) between the initial position of the bar
400   and the position encoded by each cortical image pixel (**Figure 4D** bottom panel). Responses
401   peaked (triangles) at a fixed delay along the bar trajectory, dynamically mapping the bar motion
402   with the accurate speed (6.8dva/s), corresponding to a cortical speed of 0.016m/s (the equivalent

13

403   of v_{ff} in our model). Notice that, in **Figure 4D** we aligned the responses to the end of the
404   trajectories, hereby correcting for bar motion. As a consequence, the vertical alignment of peaks
405   demonstrates that it always occurs when the bar was at the retinotopic position encoded by the
406   retinotopic map (in other words, when it reaches the population RF). In contrast, response onset
407   latencies for pixels close (<2dva) to the starting position of the bar motion decreased rapidly. By
408   fitting this spatio-temporal profile as in the model, we estimated an apparent cortical speed of
409   0.06m/s, consistent with the speed of intra-cortical horizontal propagation (Bringuier et al., 1999;
410   Girard et al., 2001; Muller et al., 2014; Reynaud et al., 2012). This result suggests that intra-
411   cortical inputs, propagating faster on the cortex than the feedforward activation sequence elicited
412   by the moving bar (0.06 vs 0.016 m/s), is most probably at the origin of the anticipatory
413   activation observed in macaque area V1.

414

415   However, for pixels located more than 2dva away from the stimulus starting position (i.e. the
416   position is estimated from the piecewise linear regression fit procedure), responses latencies
417   decreased much less, corresponding to a cortical speed of ~0.02m/s. Such temporal dynamics
418   corresponds to a visual speed of 8.8dva/s, only slightly higher than the bar translation speed
419   (6.6dva/s). Accordingly to our model, such values suggest that the large anticipatory responses
420   seen for long distances, result from the sequential activation of a nested horizontal network
421   driving responses with a spatial range of 2dva. It is compatible with the spatial extent of the
422   horizontal network in macaque V1 (Angelucci et al., 2002). These measured values for both
423   speed and spatial extent are compatible with the intra-cortical connectivity but not with a
424   feedforward origin. Indeed, if anticipation would result from divergence of the feedforward
425   network, our model predicts a faster latency decrease and the spatial extent of this decrease
426   would be smaller than the one we measured (Blasdel and Lund, 1983; Florence et al., 1988;
427   Perkel et al., 1986). Overall, both model prediction and VSDi measurements are in strong
428   agreement to support an intra-cortical origin of anticipatory responses in macaque V1.
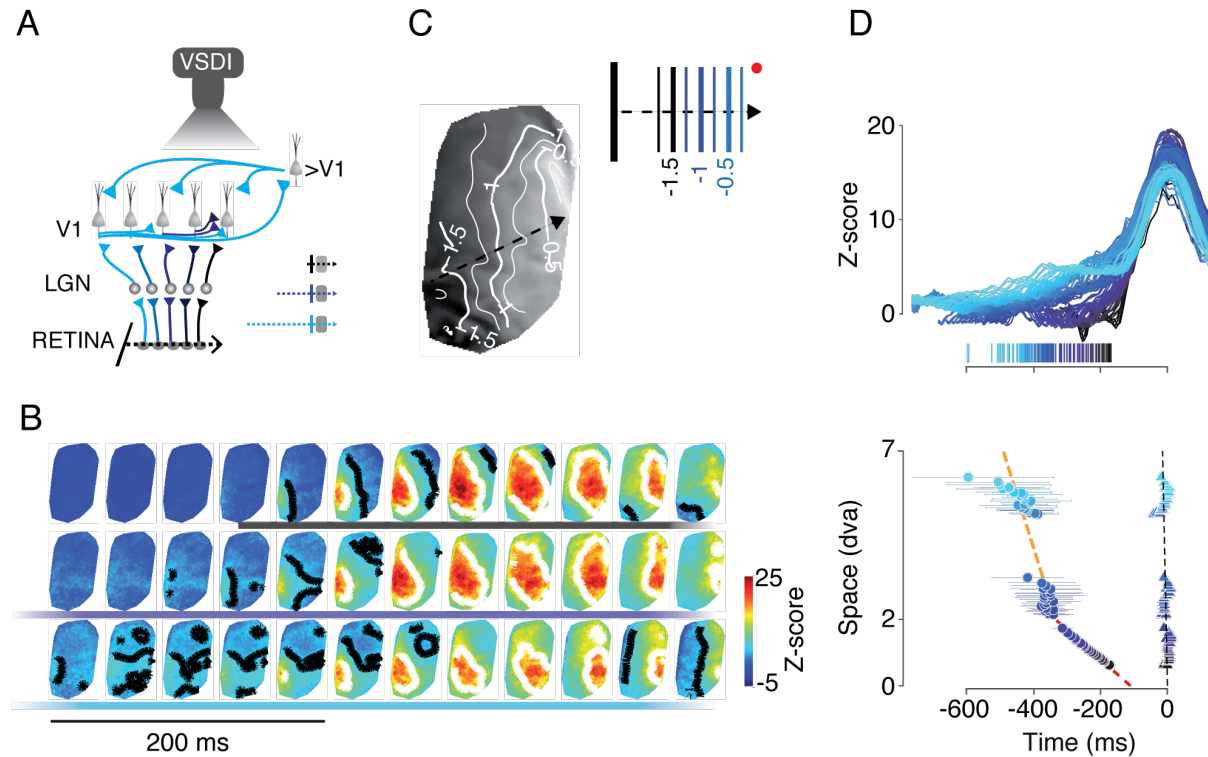
429

Figure 4. Neural population responses to a translating bar as a function of trajectory length

(A) Experimental rationale. Similar to Figure1A but VSD responses are captured using a CCD camera. **(B)** Time sequence of the VSD response map (2 sessions, n=37 trials) for the three trajectory conditions. **(C)** Retinotopic map of the horizontal dimension (grayscale code for the horizontal eccentricity, contours delimit the progression for every 0.5dva). Top-right: Cartoon representing corresponding bar positions in the visual field in the blue color-code. **(D)** Top: Time course of the VSD responses for all conditions broken down by the distance of the initial bar position to the pixel's retinotopic position. Vertical lines: responses latencies. Color-code same as Figure3C. Bottom: Latency (circle) and time-to-peak (triangle) of VSD responses as a function of the distance of the initial position of the bar to the retinotopic representation (similar to Figure 3C). Red and orange lines are linear regressions.

What could be the origin of the difference observed between cortical (8.8dva/s) and stimulus (6.6dva/s) speeds? One hypothesis is that it result from gain modulation exerted by long-distance feedback inputs, since only those can mediate such long-range lateral interactions (Angelucci et al., 2002). Therefore, we added a feedback component to our model that acts by varying the relative gain between horizontal and feedforward inputs, as already suggested by others (Liang et al., 2017; Piech et al., 2013; Ramalingam et al., 2013). Increasing the gain of lateral inputs changed the shape of the response time-course (**Figure 3F**) resulting in an increased detectability of the response and, thereby, slightly increasing the slope of the second component in our spatiotemporal profile. These effects are consistent with the results obtained in VSD. To verify this hypothesis, our next step was to test whether the time-scale of such gain modulation was coherent with the dynamics of feedback inputs.

15

Low-frequency LFP signals support the existence of an early and diffuse anticipation signal

Convergent studies have recently suggested that the power of low-frequency (i.e. alpha and beta bands) local-field potentials (LFP) signals in V1 can be used as a proxy to quantify the amount of feedback inputs onto V1 (Bastos et al., 2014; van Kerkoerle et al., 2014). Therefore, in order to test our model prediction, that the contribution of feedback signals could participate to the dynamic of anticipatory responses, we studied the time-course of low-frequency LFP signals in V1 in response to our 3-trajectories paradigm (**Figure 5A**). To do so, we measured LFP signals from arrays of 10x10 electrodes (Utah arrays, **MEA**) chronically implanted in two monkeys (BA and PD). The arrays covered a V1 cortical territory of 4x4mm, representing 2-3dva of the motion path. Similar to VSDi, the LFP response (0.3 - 250Hz) to the translating bar across the array followed the projection of the bar to the retinotopic map, swiping across the cortex at the matching cortical speed of 0.015m/s (**Figure 5B**).

For longer trajectories (lower rows), clear anticipatory LFP responses were observed all over the array. As for above, we aligned the responses from all electrodes based on their retinotopic position and calculated the time-course of the LFP power-frequency spectrum for the responses to the three trajectories conditions (**Figure 5C**). The anticipatory response was evidenced as a power increase or decrease at high or low frequencies, respectively. Across all frequencies, the response peak always occurred when the bar crossed the centre of the retinotopic area covered by the electrodes array. To detail the dynamics of low and high frequency LFP signals as a function of the bar trajectory length, we filtered the LFP responses using two bandwidths (low: bandwidth 7-25Hz and high: 40-100Hz) and aligned these signals based on the distance between the RF position for each electrode and the initial position of the trajectory (**Figure 5D-E,** top panels). We found a very early and strong anticipatory decrease in the low frequency band. At higher frequencies, however, the anticipatory build-up was more similar to the spiking activities described above, both in terms of amplitude and latency. For both frequency bands, changes were graded according to the length of the motion path. To interpret these results in the framework of our model, we extracted the latency of low- and high-frequency bands and plotted them as a function of trajectory length (**Figure 5D-E**, bottom panels). At high frequencies, in the gamma-band regime, we observed a dynamic similar to single-units and VSDi with an initial phase of latency decrease well captured by a propagation of 0.14m/s. For distances larger than 2dva, the decrease in latency is stable. However, at low-frequencies, in the alpha to beta-band regimes, we observed a constant delay after stimulus onset for all trajectories.

This temporal dynamic could be due to divergent inputs from either thalamo-cortical or feedback pathways, since both can generate synchronous inputs over a large extent. However, given the limits on the spatial extent of the thalamic axonal arbors in primates (less than 0.5mm, (Blasdel and Lund, 1983; Florence et al., 1988; Perkel et al., 1986)) and the divergence of thalamo-cortical inputs (less than 0.5mm in diameter, (Perkel et al., 1986)), this effect is more probably due to feedback from downstream areas that, in contrast, have the appropriate spatial and

493   temporal scales (Angelucci et al., 2002; Girard et al., 2001; Stettler et al., 2002). Overall, these
494   results are consistent with the predictions of our model. In the last part of our study, we further
495   support the hypothesis that the generation of anticipatory responses necessitates lateral
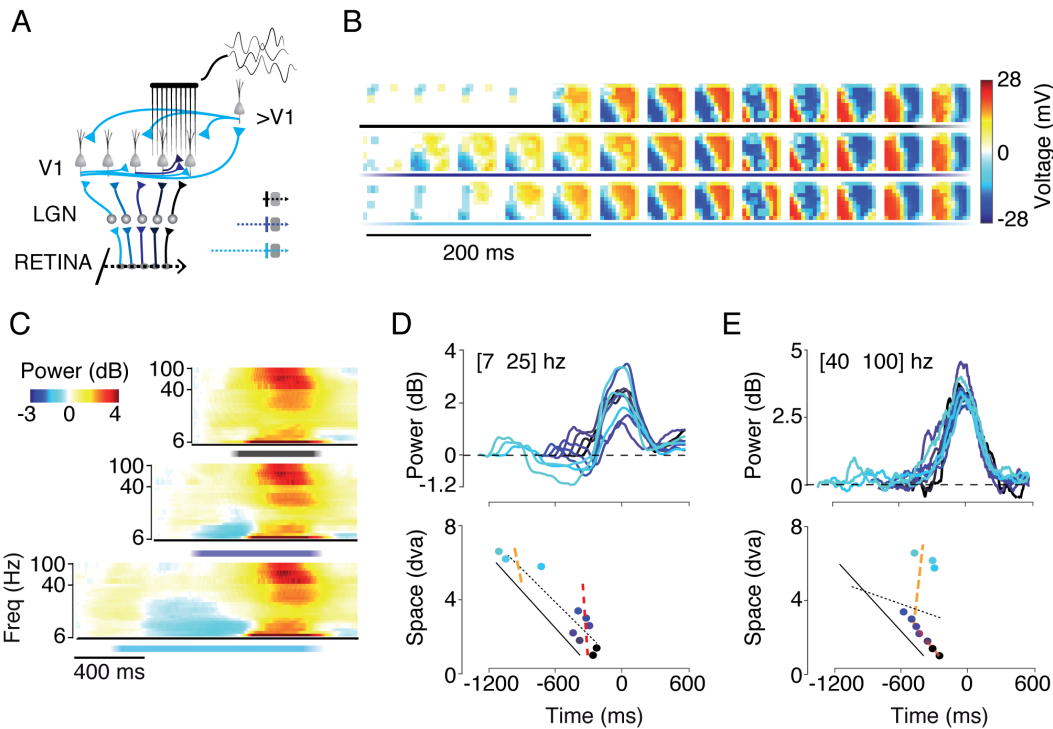496   propagation of activity using a complementary approach.

497
498

Figure 5. Multi-unit LFP responses as a function of stimulus' trajectory length (**A**) Experimental
approach. Similar to Fig. 1A but the LFP of the neural population response is recorded using a square
multi-electrode-array (MEA) (**B**) Time sequence of the map of LFP responses in MEA space for the three
trajectory lengths, (3 sessions, 52 trials per condition). Colored lines at the bottom indicate stimulus
presentation and condition type (color-code) (**C**) Time-frequency representation of the LFP power
averaged across 96 electrodes. (**D-E**) <u>Top:</u> Time-course of the averaged LFP power for low (D) and high
(E) frequency bands, for all conditions broken down by the distance of the initial bar position to each
electrode retinotopic position (t=0ms). Black-to-cyan color codes for the increasing distance of the
electrode retinotopic position to the initial position of the bar. <u>Bottom:</u> Latency (circle) of LFP responses
as a function of the distance of the initial position of the bar to the retinotopic representation. The black
line corresponds to the bar trajectory time-course. The orange and red dotted lines are the result of a
piecewise linear regression and the black dotted line of a single linear regression.

511
512

Anticipation is cancelled for inter-hemifield stimulation

513   In all conditions tested so far, bar trajectories were all presented in the contra-lateral visual hemi-
514   field, activating a continuous cortical path confined within the recorded hemisphere. If the intra-
515   cortical origin hypothesis holds true, anticipatory responses should not be evoked when the
516   trajectory has its origin within the ipsilateral visual hemifield. This is due to the fact that, since
517   our recordings are retinotopically located very close to the vertical meridian, such stimuli would

519   activate first the opposite hemisphere, generating activation to the recorded location through the
520   myelinated callosal V1-V1 connections, that are much faster than the amyelinated lateral
521   connections and are mostly restricted to a region close to the vertical meridian (Kennedy and
522   Dehay, 1988; Kennedy et al., 1986).

523

524   In three monkeys, we tested this prediction using both LFP (**Figure 6A**) and VSDI recordings
525   (**Figure 6B**). As expected, for the opposite stimulus direction, the peaks of the LFP and VSDi
526   responses move towards the opposite cortical direction (compared to **Figures 4** and **5**). However,
527   in stark contrast to a stimulus restricted to the contra-lateral hemi-field (**Figures 4,5**), moving a
528   visual stimulus from the ipsi-lateral hemifield did not generated anticipatory responses, for both
529   types of recordings and for both low and high frequency power values (see below). This result
530   provides another strong evidence that the observed anticipatory responses are mainly driven by
531   propagations within the intra- an inter-cortical, horizontal and feedback networks.
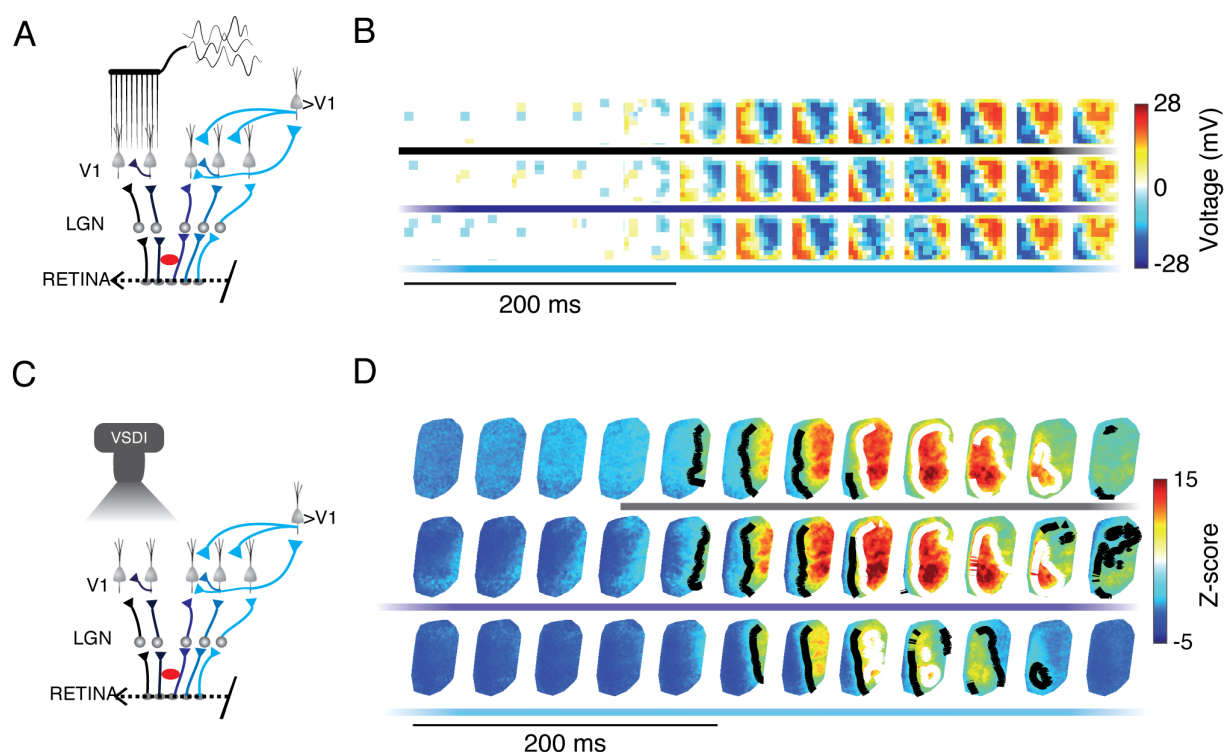
532

533

Figure 6. Neural population responses to trajectories with different lengths presented in the ipsi-lateral visual hemi-field. (A,C) The experimental rational for LFP (A) and VSDi (C) recordings. Neural responses are measured in the retinotopic area close to the vertical meridian for a bar starting to move from the ipsi-lateral visual hemifield (i.e. activating the opposite hemisphere) and finishing its trajectory just after crossing the vertical meridian (i.e. activating the recorded hemisphere). Red discs indicate the position of the fixation spot. **(B)** and **(D)** same legend as in Figure 4B and 5B respectively.

540

541 Lastly, we compared the average responses latencies across all monkeys, for the three
542 complementary recordings, the three different trajectory length and the two trajectory directions
543 (**Figure 7**). For a stimulation within the contra-lateral hemifield, anticipation gradually develops
544 along the trajectory length in the various measures of neuronal activity. The strongest
545 anticipation was seen for low-frequency band LFP responses (squares), followed by VSDi
546 (triangle) and high-frequency LFP (diamond) responses, leading to a final anticipation expressed
547 at suprathreshold level in single unit activity (circle, **Figure 7A**). For the opposite direction, in
548 both LFP and VSDi recordings, no sign of anticipation is evident for both LFP and VSD signals.
549 Moreover, delayed responses are observed in the VSDi responses for the long trajectories.
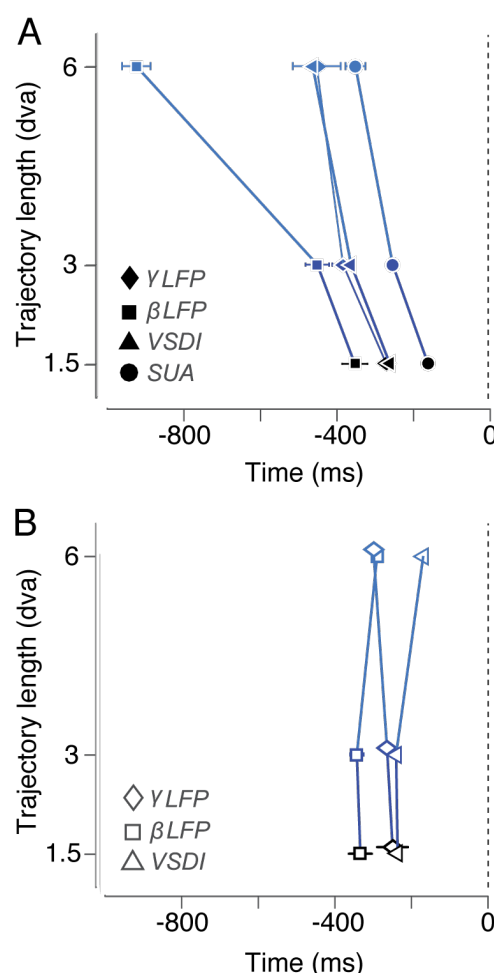550 (**Figure 7B**).

551

552

553 **Figure 7. Comparison of results across all recording techniques and 4 monkeys.** (**A**) Averaged
554 latencies of SUA (2 monkeys), LFP power and VSDi responses as a function of trajectory length for
555 stimulation within the contra-hemifield. (**B**) Same than A but for a bar coming from the ipsi-lateral
556 hemifield. SEM is calculated across all neurons (SUA) electrodes (LFP) or pixels (VSD).

557

DISCUSSION

In primary visual cortex of awake, fixating monkeys, we show that a bar translating along a smooth and extended trajectory significantly activates half of the recorded neurons several hundreds of milliseconds and a few degrees before actually entering their classical RF. This trajectory-dependent anticipatory activity has a specific slow temporal profile composed of a ramping response that is intrinsically different from the classical transient and fast responses driven by pure feed-forward cortical inputs. Such anticipatory activity cannot be explained by an underestimation of the RF sizes or by the scatter in the eye positions. These surprising anticipatory spiking responses present a wide range of timings across neurons, longer trajectory lengths leading to earlier response build-up onsets. This variability in anticipatory response onset is partially accounted for by the neurons' direction preference: cells preferring the motion direction of the bar display the strongest and earliest anticipatory build-up of spiking activity. In contrast, after entering the classical RF of the neurons, the translating bar produces the same spiking activity regardless of its trajectory length and therefore its cortical mapping history.

Anticipatory responses in the visual system have already been reported in a few physiological studies, first in vitro in the retina of rabbit and salamander (Berry et al., 1999), in area 17 of anesthetized cat (Jancke et al., 2004b; Orban et al., 1985), but also monkeys areas V1 (Guo et al., 2007; Subramaniyan et al., 2018) and V4 (Sundberg et al., 2006). However, these previous observations all differ on several key features when compared to our present study. First, these previous studies (with the exception of Guo et al., 2007, see below) were inspired by the flash-lag effect, in which a translating stimulus is judged ahead of a stimulus flashed at the same position at the same time. In this context, these studies have compared the latency of responses evoked by bars in translation to bars flashed alone in the RF centre. The RF was therefore stimulated differently by the flashed and the moving stimuli, in the sense that the moving stimulus activated a sequence of positions in the RF before reaching the position in which the flashed stimuli was presented for comparison. In contrast, in our approach, the classical RF is stimulated exactly in the same way for all trajectory conditions. Consistent with their initial hypothesis, these previous studies showed a global shift in the time-course of their responses, while maintaining the same shape (i.e. time-to-peak and response offset present similar anticipation than response onset). In our study, anticipatory responses consist in the appearance of an early ramping activity for long trajectory. Afterwards, the response peaks and decrease at the same time than shorter trajectories.

Our results are in accordance with an earlier study carried out in the anesthetized macaque on a small number of neurons, where a bar flashed just outside the classical RF of a V1 neuron can evoke a response when presented after a sequence of 3 other collinear bars in apparent motion, outside the RF (Guo et al., 2007). However, the phenomenon reported in this study is again different from the one we report, since the apparent motion stimulus used will stimulate V1 in a sequence of discrete and transient feedforward activations, creating an intrinsically different

598   activity pattern than that caused by a smooth translating stimulus. Indeed, it has been recently
599   demonstrated, using VSDi in the awake monkey, that a two-strokes apparent motion stimulus
600   generates two waves of propagation interacting non-linearly, instead of many cumulative
601   propagations produced by each position visited by a translating object (Chemla et al., 2019).
602

603   Crossing different physiological signatures at single cell and population levels, and guided by a
604   computational model, we provide convergent evidence that the observed spiking anticipation is
605   not a mere consequence of similar events occurring at earlier processing stages but rather results
606   from a specific propagation of activity within V1 intra- and inter-cortical networks. Our
607   biologically realistic-model shows that the cumulative recruitment of converging horizontal input
608   can produce a gradual build-up of anticipatory activity preceding the feedforward activation.
609   Such build-up is evident at both sub-threshold and spiking levels. The trajectory-dependent shift
610   in response onset timing was also observed with high resolution and large field-of-view using
611   VSDi. From the time-course of these neural population responses across the retinotopic map, we
612   have been able to estimate the speed and spatial extent of the propagation underlying the
613   observed anticipation. The spatio-temporal properties of such propagation are fully compatible
614   with the well-known characteristics of the cortical horizontal network in primate area V1 for
615   trajectories up to 2dva (Angelucci et al., 2002; Girard et al., 2001; Muller et al., 2014).
616

617   On the other hand, the further decrease in the response onset we observed using VSDi for
618   trajectories extending beyond 2dva (i.e. covering more than 6mm of cortical space) cannot be
619   explained by this horizontal network alone because of the limitation in horizontal connections
620   length. Therefore, we hypothesized that a divergent feedback input from higher visual areas
621   could generate such fast and long-distance effect (Angelucci and Bressloff, 2006; Bair et al.,
622   2003; Bullier, 2001). Using our model, we found that a feedback mechanism can indeed induce a
623   further, though smaller, decrease of response onset for these larger trajectory distances, as
624   observed with VSDi. To support this hypothesis, we show that the bar appearance, even for
625   trajectories longer than 2dva, triggers a fast and strong decrease of low-frequency LFP power,
626   that is likely to indicate a feedback modulation (Bastos et al., 2014; van Kerkoerle et al., 2014).
627   Furthermore, the spatial and temporal properties of this signal are compatible with the known
628   properties of the feedback connectivity (Angelucci and Bressloff, 2006; Bair et al., 2003; Bullier,
629   2001; Girard et al., 2001). As suggested for sensory-motor networks, such decrease could be
630   related to reporting an expected change in the input, a deviation from the "status quo" (Engel
631   and Fries, 2010).
632

633   A last and strong piece of evidence in support of the intra-cortical propagation mechanism comes
634   from our control experiment in which we moved the bar from the ipsilateral visual hemifield,
635   first activating the cortical hemisphere opposite to our recordings. In fact, while slow lateral
636   interactions, mediated by amyelinated horizontal connections, are restricted to the same
637   hemisphere, inter-hemispheric interactions, mediated by fast myelinated callosal connections, are

638   restricted to a region of the visual field close to the vertical meridian (Kennedy and Dehay, 1988;
639   Kennedy et al., 1986). Therefore, a bar moving within the ipsi-lateral visual hemifield would not
640   activate the horizontal network of the recorded cortex. Fast, inter-hemispheric callosal
641   interactions will signal the arrival of the bar in the contra-lateral visual hemifield but only when
642   it approaches the vertical meridian and without any precise retinotopic projection. This is
643   consistent with fact that we did not observe any anticipatory responses in our population activity
644   measurements (VSDi, LFP) for ipsi-lateral approaching bar. While we did not record single unit
645   activities under this condition, VSDi and gamma power LFP signals indicate also the presence of
646   spiking activities. We shall therefore not expect to find any significant slow ramping of spiking
647   activity when a moving object approaches from the other side of the vertical meridian. This does
648   not preclude, however, that inter-hemispheric trajectories could be linked at other spatio-
649   temporal scales in extra-striate cortex that can exhibit larger receptive fields with ipsilateral
650   representations (Desimone et al., 1993; Gross et al., 1977; Pigarev et al., 2001).

651

652   All these converging evidences thus suggest that trajectory-dependent, anticipatory, spiking
653   activity results from the interplay of intra- and inter-cortical networks, both propagating activity
654   faster than the feedforward sequence of inputs. Incidentally, our results also show that, through
655   the accumulation of convergent sub-threshold activations, intra-cortical network can drive
656   spiking responses several hundreds of millisecond before the arrival of feedforward inputs,
657   instead of being only modulatory (see also (Jancke et al., 2004a). A possible functional
658   consequence could be that V1 neurons can signal the direction of a moving object before it
659   reaches their receptive fields. Indeed, the fact that anticipatory responses are stronger for neurons
660   whose direction preference matches the trajectory motion direction suggests that direction-
661   selective anticipatory signals can reach downstream populations of neurons (for example MT
662   cells). Thus, motion integration might be facilitated by propagation of anisotropic and
663   anticipatory signals, alleviating motion uncertainties (Burgi et al., 2000; Perrinet and Masson,
664   2012; Tlapale et al., 2010).

665

666   Our study documents for the first time that the neural activity evoked along the trajectory travels
667   across the retinotopic map at the cadence imposed by the FF response, representing at each
668   moment in time information about the stimulus recent history but also its likely future location
669   and velocity. The cortical representation of the leading edge of a motion trajectory is gradually
670   spreading out over a larger retinotopic area than stimuli presented along short trajectories.
671   Downstream extra-striate visual neurons with large RFs could therefore integrate both the
672   feedforward evoked population response with this trajectory-dependent population response.
673   This could be relevant in explaining why stimuli presented at the leading edge of motion
674   trajectories are more detectable (Arnold et al., 2014; Lenkic and Enns, 2013; Liu et al., 2006;
675   Roach et al., 2011; Schwiedrzik et al., 2007) and their location are perceived ahead of a stimulus
676   flashed in the same position (Jancke et al., 2004b; Nijhawan, 1994).

677

678 Additionally, this phenomenon could be at the origin of the diffusion of motion information, a
679 mechanism postulated to be necessary for enhancing motion discriminability (Burgi et al., 2000;
680 Grzywacz et al., 1995; Yuille and Grzywacz, 1989), and inferring non-ambiguous motion
681 direction (Anstis and Ramachandran, 1987; Perrinet and Masson, 2012; Ramachandran and
682 Anstis, 1983). Consistently with our observations indeed, such psychophysical effects are
683 modulated by motion trajectory length (McKee and Welch, 1985; Nakayama and Silverman,
684 1984; Snowden and Braddick, 1989a, 1989b; Watamaniuk et al., 1995). Hence, this circuitry
685 may serve as a plausible mechanism for a predictive coding of future locations and to resolve
686 motion integration computations (Kaplan et al., 2013; Khoei et al., 2017; Perrinet and Masson,
687 2012). Indeed, such diffusion could subserve two key computational elements of predictive
688 coding: taking advantage of temporal coherency to predict future events and removing highly
689 correlated events within the sensory inflow (Alink et al., 2010; Mumford, 1992; Rao and Ballard,
690 1999).

691

692 In conclusion, our study suggests that propagation of activity within or between cortical areas
693 may play an important role in the dynamical processing of non-stationary stimuli (see also
694 (Chemla et al., 2019; Muller et al., 2018)). We document an effect occurring at the specific
695 spatial and temporal scales of macaque area V1. The anticipatory effect propagates only over a
696 few degrees ahead of the translating bar. We shall envision that the lateral interactions will
697 propagate information across the overlaid functional maps not only in V1, but also in all the
698 other visual areas and maps. In other words, we may imagine a generalization of the effect across
699 the various scales of the encoded retinotopic maps along the visual system, or across different
700 feature maps such as the orientation map in V1 (Chavane et al 2011, Rankin & Chavane 2016,
701 Tlapale et al, 2010), the direction map in MT (DeAngelis and Newsome, 1999) or more complex
702 maps in other extra-striate visual areas. Analyzing systematically the anticipation across these
703 feature maps may help to understand to what extent this anticipatory signal is a simple predictive
704 warning signal or whether it carries more information about the nature of the incoming stimulus.
705 We propose that parallel propagation of information within all these maps, combined with rapid
706 exchange of information between these maps, may be a canonical computational operation by
707 which the visual system process complex, natural, non-stationary inputs.

708
709
710

711 **METHODS**

712 **1. Animals and surgery procedures**

713

714 Experiments were conducted on a total of five hemispheres, in four adult male rhesus monkeys
715 (*Macaca mulatta):* monkeys NO (right hemisphere), PD (left and right), BM (right), BR (right).
716 Experimental protocols have been approved by the Marseille Ethical Committee for Animal
717 Research (approval #A10/01/13, official national registration #71-French Ministry of Research).

All procedures complied with the French and European regulations for animal research, as well as the guidelines from the Society for Neuroscience. All the monkeys were chronically implanted with a head-holder. Monkey NO, PD and BR were also implanted with a recording chamber located above areas V1/V2. Monkey PD and monkey BM were implanted with a Utah array. Monkey BR had a third surgery for durotomy and transparent artificial dura mater insertion, in order to perform voltage-sensitive dye imaging. Monkeys NO and PD were implanted with a scleral search coil for right eye position monitoring.

Multi-electrodes array: Ninety days after head holder implantation, once monkeys PD and BM were trained to achieve a good fixation, a second surgery was performed. Area V1 of the left (monkey PD) and the right hemisphere (monkey BM) were surgically implanted with a 100-electrode Utah array (Blackrock Microsystems, Salt Lake City, UT, USA). The array had an arrangement of 10×10 (PD: Platinum $\sim 400 k\Omega$ 1kHz, BM: Iridium oxide $\sim 50 k\Omega$, at 1kHz) electrodes, each of them 1mm long, with an inter-electrode distance of 400μm. The surgery was performed under deep general anesthesia and full aseptic procedures. Anesthesia was induced with 10mg/kg *i.m*. ketamine and maintained with 2–2.5% isoflurane in 40:60 O2–air. To prevent cortical swelling, 2ml/kg of mannitol *i.v*. was slowly injected over a period of 10min. A 2×2 cm craniotomy was performed over the visual cortex and the dura was incised and reflected. The Utah array was inserted in the cortex using a pneumatic inserter (Array Inserter, Blackrock Microsystems) ~5mm under the lunate sulcus, in perifoveal position and covered with a sheet of an artificial non-absorbable dura (Gore-tex). The real dura was sutured back and covered with a piece of an artificial absorbable dura (Seamdura, Codman). The bone flap was put back at its original position and attached to the skull by means of a 4×40 mm strip of titanium (Bioplate, Codman). The array connector was fixed to the skull on the opposite side with titanium bone screws (Bioplate, Codman). The skin was sutured back over the bone flap and around the connector. The monkey received a full course of antibiotics and analgesic before returning to the home cage.

Voltage sensitive dye imaging (VSDi): The surgical preparation and VSD imaging protocol have been previously described in Reynaud et al., 2012 (Reynaud et al., 2011). Briefly, after head holder and chamber implantation on the right hemisphere, a second surgery was performed, once the monkey BR was trained to achieve a good fixation. The dura was removed surgically over a surface corresponding to the recording aperture (18mm diameter), and a silicon-made artificial dura was inserted under aseptic conditions (Arieli et al., 2002). Such silicon-dura is necessary to have a good optical access to the cortex.

2. Recordings

Eye Movements: For monkeys NO and PD, horizontal and vertical positions of the contra-lateral eye to the recorded hemisphere, were recorded using the scleral search coil technique

758 (Judge et al., 1980; Robinson, 1963). For those monkeys, a second surgery was performed to
759 insert a search coil below the ocular sclera, to record eye movements with the electromagnetic
760 technique (Robinson, 1963). For monkey PD and BM we used the Eyelink 1000 (SR Research
761 sampling frequency of 1,000Hz). For monkey BR, we used an ISCAN eye tracking system (512
762 x 256 x 60Hz, ETL-200).

763

764 **Single electrode (SE):** A computer-controlled microdrive (MT-EPS, AlphaOmega, Israel) was
765 used to insert through the dura a tungsten micro-electrode (FHC, 0.5-1.2MΩ at 1,000Hz) on the
766 right hemisphere of monkey PD and NO. Spikes were sorted on-line using a template-matching
767 algorithm (MSD, AlphaOmega).

768

769 **Multi-electrodes array (MEA):** Recordings were carried out through a 128-channel Cerebus
770 acquisition system. The signal from each active electrode (96 out of the 100 electrodes were
771 connected) was pre-processed by a head stage with unity gain and then amplified with a gain of
772 5000. The signal was filtered in two different frequency bands to split it into LFPs (0.3–250Hz)
773 and spiking activity (0.5–7.5kHz). The LFPs were sampled at 1kHz and saved on disk. To
774 improve the electrode independence among LFPs, we subtracted from all electrodes the common
775 LFP averaged across all electrodes.

776

777 **Voltage sensitive dye imaging (VSDi):** After removing of the artificial dura-mater, the cortex
778 was stained with the voltage-sensitive dye RH-1691 (Optical Imaging), prepared in artificial
779 cerebrospinal fluid (aCSF) at a concentration of 0.2mg/ml, and filtered through a 0.2µm filter.
780 After a 3 hours staining period, the chamber was rinsed thoroughly with filtered aCSF, to wash
781 off any supernatant dye. The artificial dura was inserted back and the chamber closed with
782 transparent agar and cover glass. Optical signals were recorded from a focal place ~300µm
783 below the surface using a Dalstar camera (512x512pixels resolution, frame rate of 110Hz) driven
784 by the Imager 3001 system (Optical Imaging). Excitation light was provided by a 150W halogen
785 lamp filtered at 630nm and fluorescent signals were high-pass filtered at 665nm during 1363ms
786 (trial duration).

787

788

789

790 **3. Experimental protocols**

791

792 **Behavioral task and Training:** Monkeys were trained to fixate a red target presented on the
793 center of the screen for all the duration of the trial (~1.5sec) within a window of 1-2dva of
794 diameter. We monitored the eye positions and controlled online the behaviour (sampling rate: 1
795 KHz) using the REX package under the QNX operating system (Hays et al., 1982). For VSDI
796 experiments, both online behavioral control and image acquisition were heartbeat triggered;
797 heartbeat was detected with a pulse oximeter (Nonin 8600V). After a successful trial, i.e. the

798 monkey has maintained his fixation during the whole acquisition period (~2s), monkeys received
799 a drop of water (NO, PD, BM) or mashed apple (BR) as a reward. For VSDi recordings, an inter-
800 trial interval of 8 sec was set for dye bleaching prevention.
801
802 **Visual stimulation:** Visual stimulation protocols were displayed using different devices
803 depending on the technique. For both SE and MEA recordings, they have been produced using
804 in-house software (Gérard Sadoc, Acquis1-Elphy, Biologic CNRS-UNIC/ANVAR) but with
805 different displays. In each system, the display was gamma calibrated by means of a lookup table.
806 For the SE experiments, stimuli were back-projected on a translucent screen covering of visual
807 field of the monkey, at a distance of 100 cm, using a video projector (resolution:
808 1280×1024 pixels at 60 Hz, operating range 0-24 cd/m^2). The luminance of the motion stimulus
809 was 22.2 cd/m^2 (background 2.2cd/m^2). For the MEA experiments, stimuli were presented on a
810 LCD screen 27' (resolution: 1920x1080 pixels at 60Hz, operating range 0-294cd/m^2) at a
811 distance of 57cm. Mean luminance of the motion stimulus was 80cd/m2 (background 5cd/m^2).
812 For VSDI, the visual stimuli were computed on-line using VSG2/5 (VSL v8) libraries on Matlab
813 (The MatWorks Inc., Natick, MA, USA) and were displayed on a 22' CRT monitor at a
814 resolution of 1024x768 pixels and a refresh rate of 100Hz, operating range 0-75cd/m^2. The
815 viewing distance was set to 57cm, the mean luminance of the motion stimulus was set to
816 71cd/m2 and the background was kept constant to 12cd/m^2
817
818 **SE stimulation protocol:** Each neuron was characterized using three different stimulation
819 paradigms. First a sparse noise (SN) paradigm, to quantitatively map out the receptive field (RF)
820 of the neuron. The SN consisted in the sequential presentation of small dark and light squares of
821 0.6x0.6dva, flashed for 50ms randomly positioned within a 10x10 grid (11.2+/-11 cd/m2,
822 ~15trials, see (Bringuier et al., 1999). The stimulation for the following paradigms was centered
823 on the RF centre (RFc). To estimate the RFc, we extracted the center from the ellipse that was
824 best adjusted to the activity contour at a 3.8 z-score (equivalent to a p-value of 0.1% corrected
825 for 100 positions). Then, a direction tuning (DT) paradigm, using a bright bar (0.5 x 4 dva)
826 moving at 6.6 dva/s. The bar was crossing the stimulation centre in the middle of its trajectory (6
827 dva altogether) and randomly presented at 12 different directions (spaced by 30° of circular
828 angle). The bar orientation was always perpendicular to the motion direction. Finally, a trajectory
829 length paradigm (3T) in which the same bar, oriented perpendicularly to the motion direction
830 was moved horizontally at 6.6 dva/s, starting at 1.5, 3 or 6 dva from the RF centre and
831 disappearing 1.5 (NO) or 2 dva (PD) beyond the RF centre. The bar trajectory started from a
832 lateral position in the contra-lateral visual hemi-field towards the vertical meridian. In those three
833 protocols, control trials with no stimulation were presented within each block (blank condition).
834 All stimuli were presented in random order.
835
836 **MEA stimulation protocol:** Electrodes LFP RF were mapped by the same sparse-noise
837 paradigm used for SE and stimulation was centered on the centre of mass of the population RFs.

838   Then, we used the same protocols (DT and 3T) than for single units recordings. However, we
839   also extended the protocol 3T using a symmetrical trajectory moving towards the RFs from the
840   ipsilateral visual hemi-field.

841

842   **VSDi stimulation protocol:** The VSDi stimulation protocol for the 3T paradigm was established
843   using the exact same stimuli (see above). The trajectory vertical position was centered on 2dva
844   below the horizontal, the imaging area being roughly centered on [-2; -1dva] (see retinotopic
845   map using intrinsic optical imaging Figure 4C), while horizontally moving at 6.6dva/s from 7, 4
846   or 2.5dva on the left of the vertical meridian to 0dva (vertical meridian position). Here again, we
847   extended the protocol using a symmetrical trajectory moving towards the RFs from the ipsilateral
848   visual hemi-field. In addition to these three evoked conditions, two blank conditions, i.e. a grey
849   screen is presented during the acquisition period, were used and all stimuli were randomly
850   interleaved.

851

852   **4. Data Analysis**
853   All data have been analyzed using custom-written routines in Matlab.

854

855   **SUA PSTH plots:** For every neuron, we calculated the peristimulus time histograms (PSTH) for
856   the three trajectory lengths conditions, averaging across the trials PSTHs (total number of trials
857   between 15 and 35, bin size of 10ms), smoothed by a low pass filter (window of 120 ms) and
858   expressed in spikes per second. Standard error of the mean (SEM) was calculated across trials.
859   First, the histogram of every trial (bin size 10ms) was smoothed with a low pass filter (window
860   of 120ms). Then we calculated the SEM across these smoothed histograms. Response latency
861   was calculated on PSTHs that had a peak response higher than 1.96 times the standard deviation
862   over the mean of the amplitude of the blank condition PSTH (amplitude threshold). The latency
863   was computed on the PSTH derivative (estimated on each time frame "t" by calculating the
864   linear regression of the PSTH response over 20 points, corresponding to 200ms, centred on t).
865   The latency was defined on each condition as the moment the PSTH derivative was crossing a
866   threshold, (calculated as the mean plus 1.96 times the standard deviation of the derivative of the
867   blank condition PSTH) for 5 consecutive points.

868

869   **Averaged PSTHs:** For each monkey, we averaged the PSTHs of cells presenting a statistically
870   significant anticipatory response (two-sample t-test between the distribution of spikes numbers
871   for trial of the longer trajectory length conditions and the short one in a 100ms time window
872   placed just before the response latency for the short trajectory, i.e. just outside the classical RF).
873   Before averaging, single cells PSTHs were aligned on the latency of the short trajectory
874   condition. Second, to remove the unselective component of the response for each cell, the
875   average across time of the PSTH baseline (the first 400ms before stimulus presentation) was
876   subtracted from the full PSTH. To align the PSTHs of each cell on the latency for the short
877   trajectory, for each condition, we first calculated the error between the expected (40ms after

27

878 stimulus presentation) and measured latency and then we adjusted the PSTHs offset in time to
879 remove it. The statistical significance of the averaged responses was calculated over time (within
880 a sliding time window of 100ms, shifted of steps of 10ms). For each neuron and each condition,
881 the distribution of spikes counts across trials, in each time window, was compared by a two-
882 sample t-test (P<0.05) to the distribution of spikes counts across trials, over all the time windows
883 in the blank condition.

884

885 **Time course of the neurons proportion with statistically significant response:** For each
886 neuron, we calculated at which moment in time (within contiguous time windows of 100ms) the
887 distribution of spikes counts across trial, for the evoked conditions, was significantly different
888 from the distribution of spikes counts across trials and all the time windows of the blank
889 condition (one-tailed two-sample t-test, P<0.05). For each time window, we calculated the
890 percentage of neurons with a significant response, with respect to the number of neurons
891 presenting a significant response in the time window corresponding to the RF center (49
892 neurons).

893

894 **Relative firing rate within a window of 100ms just before and just after the RF border:** For
895 each neuron, we calculated the difference in spike rate between the short and the longer
896 trajectories conditions (aligned on the RF centre) within a 100ms window, placed just before the
897 response latency if the response to the short trajectory or just after. The statistically significant
898 response differences between the distribution of spikes numbers for trial of the longer trajectory
899 length conditions and the short one, were calculated by one-tailed two-sample t-test (P<0.05).

900

901 **Neurons preferred direction and direction index:** Neurons preferred direction was calculated
902 fitting the neurons tuning curves (built from the PSTH responses within a time window of 200ms
903 centred on the RF centre for all the 12 conditions of the DT paradigm) with a double
904 multiplicative Von Mises function, see (Swindale, 1998). Neuron direction index was calculated
905 as 1, minus the ratio of the response in the opposite direction to the response in the preferred
906 direction.

907

908 **Probability of anticipation:** Probability of anticipation was calculated for each cell by one-
909 tailed two-sample t-test (P<0.05) between the short and the longer trajectory conditions (aligned
910 on the latency for the short trajectory condition) within a 100ms window place just before the
911 response latency for the short trajectory.

912

913 **Spikes representation in visual space corrected by eye position deviation from the fixation**
914 **point (control):** For 22 cells in monkey PD, we checked whether the response anticipation could
915 be explained by eye movements towards the approaching bar. For that purpose, for each trials the
916 time occurrence of each spikes was converted into a visual space coordinate corresponding to the
917 stimulus position in visual space for that particular time assuming a latency of 50ms ((skp

918   timing-50) *stimulus speed). This position was then converted by a position in retinal space
919   taking into account the distance of eye position (low pass filtered across 100 ms) from the
920   fixation centre (the average across all the eye positions), at -50ms from the spike time. Then we
921   calculated the PSTHs for the evoked conditions, in space coordinates, for the rasters before and
922   after correction of spike positions.

924   **LFP power spectral analysis:** The LFP spectrum (sampling rate 1000Hz) was computed using
925   Chronux open source MATLAB toolbox (http://www.chronux.org/, multi-taper method,
926   *mtspecgramc.m* function). Taper parameters were bandwidth (W): 2.5, taper duration (T): 1,
927   integer (p) such as 2TW-p tapers are used: 2. In order to optimize the frequency/time resolution,
928   we used two different sliding time windows for low (7-25Hz) and high (40-100Hz) frequencies
929   (respectively 400ms and 150ms). The LFP spectrum of the evoked conditions was divided for
930   the mean spectrum of the blank condition (across time) and the response offset at zero frame was
931   subtracted. LFP was recorded through a Utah array in 3 sessions for a total of 52 trials for
932   condition. The spectrogram was obtained by averaging across 96 electrodes, re-aligned on the
933   LFP RF centre of every electrode, determined through the sparse-noise paradigm (as described
934   above).

936   **VSD data analysis:** Stacks of images were stored on hard-drives for off-line analysis. The
937   analysis was carried out using the Optimization, Statistics, and Signal Processing Toolboxes. The
938   evoked response to each stimulus was computed in three successive steps. First, the recorded
939   value at each pixel was divided by the average value before stimulus onset (frames 0 division), to
940   remove slow stimulus-independent fluctuations in illumination and background fluorescence
941   levels. Second, this value was subsequently subtracted by the value obtained for the blank
942   condition (blank subtraction) to eliminate most of the noise due to heartbeat and respiration
943   (Shoham et al., 1999). Finally, a linear detrending of the time series was applied to remove
944   residual slow drifts induced by dye bleaching (Chen et al., 2008; Meirovithz et al., 2010). For
945   this study, VSD data from two sessions were accumulated by registering them onto a reference
946   session (using a quadratic registration algorithm described by Takerkart et al., 2008(Takerkart et
947   al., 2008)). Then responses amplitudes were normalized to a reference condition and data were
948   *Z*-scored(Jancke et al., 2004a) for further analysis.

950   **Retinotopic maps:** To obtain a retinotopic representation, we presented the bar stimulus
951   (0.5x4dva) at 6 different static positions (from -2.5 to 0.5dva compared to the vertical meridian)
952   for 600ms (after a delay period of 200ms) and we recorded intrinsic optical imaging signals from
953   the cortical surface(Grinvald et al., 1994). Each trial consisted of 4181ms (92frames) and was
954   followed by an inter-trials interval of 5s. For intrinsic-signal imaging, the cortex was illuminated
955   with a 605nm light. Off-line analysis of intrinsic maps started with the same normalization
956   procedures than for VSD images, i.e. frames 0 division and blank subtraction) providing the
957   cortical activation profile for each static positions of the bar. Then for each pixel, we extracted

958   the mean values in each of the six cortical profiles and computed the centre of mass. The
959   retinotopic map was finally constructed after conversion into visual field positions.

960

961   **VSDI Latency estimations:** Response latency was defined as the point in time at which the
962   signal derivative crossed a threshold set at 2.57 times (99% confidence) the SD of its baseline
963   computed during a 100-ms-long window right before stimulus onset.

964

965   **Spatio-temporal phenomenological cortical Model:** The model was built to represent V1
966   activity over a 2D matrix representing retinotopic cortical space in one dimension (full extent of
967   21mm) and time in the other dimension (full extent of 1sec). In this spatio-temporal
968   representation, we modelled the feedforward input as an activation moving across the matrix at a
969   speed of v_{ff} set to 0.016 m/s (equivalent to 6.6dva/s in cortical coordinate at the eccentricity of
970   our neural recordings). At each moment, the dot-like feedforward input generated an activation
971   profile implemented as a gaussian function in the spatial domain, with a standard deviation of
972   0.42mm.

973

974   For each of these feedforward activations, we computed V1 activity as the interaction of this
975   activation with that of similarly defined horizontal and feedback maps. First, horizontal activity
976   is the result of a spatio-temporal convolution with a kernel (k_h) which is then scaled with a non-
977   linearity. The kernel is modelled as a spreading gaussian (see eq 1) for which the standard
978   deviation increases linearly with time with a celerity c and the amplitude decreases exponentially
979   with the square of time relative to τ. The weight w_h of this kernel is adjusted to account for the
980   strength of the horizontal input. The speed of the horizontal spread v_h was therefore controlled by
981   c (set by default to 0.1m/s) and the spatial extent is controlled by a trade-off between τ and c, i.e.
982   the maximum extent being reached for the latest point in time for which the horizontal activity
983   amplitude is still above baseline. As a consequence, we used the value of σ at time $t=1.5\tau$ (the
984   amplitude will have reach 10% of its maximum) as a proxy for the horizontal extent d_h (set by
985   default to 6mm)

986

987    $$k_h = \frac{\alpha(t)}{2\pi} e^{-\frac{t^2}{2\sigma(t)}} \text{ for t>=0, where } \sigma(t) = ct \text{ and } \alpha(t) = we^{-\left(\frac{t}{\tau}\right)^2} \quad (1)$$

988

989   To account for the observation that the feedforward response amplitude does not change along
990   the trajectory, the horizontal activity contribution was scaled through a sigmoid non-linearity (**S**)
991   controlled by the difference between feedforward and horizontal activities. Horizontal and
992   feedforward signals were then linearly combined with a factor of ρ.

993

994    $$V_1 = \rho ff + (1-\rho)S\left(\frac{ff-h}{g}\right)h \text{ where } S(y) = \frac{1}{1+e^{-y}}$$

995

996　Feedback effect was thereafter modelled as a spatio-temporal multiplicative gain to the
997　horizontal activity. The kernel of the feedback was similarly designed as the one for the
998　horizontal, albeit with much faster speed and larger spatial extent. The resulting activity of the
999　feedback amplified multiplicatively the activity of the horizontal activity (Liang et al., 2017;
1000　Piech et al., 2013; Ramalingam et al., 2013). The feedback strength was controlled by a scalar
1001　weight (w_{fb}) that we modulated between 0 (no feedback) and 1.2 (feedback stronger than
1002　horizontal).

1003

1004　The evolution of the expected response time-course for different positions along the trajectory
1005　can be simply read-out from the matrix representing the spatio-temporal activity. Similarly to
1006　what was done in experimental data, latency was calculated as threshold crossing of derivative
1007　above a given value (set to 0.01).

1008
1009

AUTHOR CONTRIBUTIONS

1015

ACKNOWLEDGMENTS

1022

REFERENCES

1024 Alais, D., and Lorenceau, J. (2002). Perceptual grouping in the Ternus display: evidence for an
1025 "association field" in apparent motion. Vision Res. *42*, 1005–1016.

1026 Alink, A., Schwiedrzik, C.M., Kohler, A., Singer, W., and Muckli, L. (2010). Stimulus
1027 predictability reduces responses in primary visual cortex. J. Neurosci. *30*, 2960–2966.

1028 Angelucci, A., and Bressloff, P.C. (2006). Contribution of feedforward, lateral and feedback
1029 connections to the classical receptive field center and extra-classical receptive field surround of
1030 primate V1 neurons. Prog. Brain Res. *154*, 93–120.

1031 Angelucci, A., Levitt, J.B., Walton, E.J.S., Hupe, J.-M., Bullier, J., and Lund, J.S. (2002).
1032 Circuits for Local and Global Signal Integration in Primary Visual Cortex. J. Neurosci. *22*,
1033 8633–8646.

1034 Anstis, S., and Ramachandran, V. (1987). Visual inertia in apparent motion. Vision Res. *27*,
1035 755–764.

1036 Arieli, A., Grinvald, A., and Slovin, H. (2002). Dural substitute for long-term imaging of cortical
1037 activity in behaving monkeys and its clinical implications. J. Neurosci. Methods *114*, 119–133.

1038 Arnold, D.H., Marinovic, W., and Whitney, D. (2014). Visual motion modulates pattern
1039 sensitivity ahead, behind, and beside motion. Vision Res. *98*, 99–106.

1040 Bair, W., Cavanaugh, J.R., and Movshon, J.A. (2003). Time course and time-distance
1041 relationships for surround suppression in macaque V1 neurons. J. Neurosci. *23*, 7690–7701.

1042 Bastos, A.M., Vezoli, J., Bosman, C.A., Schoffelen, J.-M., Oostenveld, R., Dowdall, J.R.,
1043 De Weerd, P., Kennedy, H., and Fries, P. (2014). Visual Areas Exert Feedforward and Feedback
1044 Influences through Distinct Frequency Channels. Neuron *85*, 390–401.

1045 Benucci, A., Frazor, R.A., and Carandini, M. (2007). Standing waves and traveling waves
1046 distinguish two circuits in visual cortex. Neuron *55*, 103–117.

1047 Berkes, P., Orban, G., Lengyel, M., and Fiser, J. (2011). Spontaneous Cortical Activity Reveals
1048 Hallmarks of an Optimal Internal Model of the Environment. Science (80-.). *331*, 83–87.

1049 Berry, M.J.I., Brivanlou, I.H., Jordan, T.A., and Meister, M. (1999). Anticipation of moving
1050 stimuli by the retina. Nature *398*.

1051 Blasdel, G.G., and Lund, J.S. (1983). Termination of afferent axons in macaque striate cortex. J.
1052 Neurosci. *3*, 1389–1413.

1053 Bringuier, V., Chavane, F., Glaeser, L., and Frégnac, Y. (1999). Horizontal propagation of visual
1054 activity in the synaptic integration field of area 17 neurons. Science *283*, 695–699.

1055 Bullier, J. (2001). Integrated model of visual processing. Brain Res. Rev. *36*, 96–107.

1056 Burgi, P.Y., Yuille, A.L., and Grzywacz, N.M. (2000). Probabilistic motion estimation based on
1057 temporal coherence. Neural Comput. *12*, 1839–1867.

1058 Burr, D., and Ross, J. (1986). Visual processing of motion. Trends Neurosci. *9*, 304–307.

1059 Carandini, M., Demb, J.B., Mante, V., Tolhurst, D.J., Dan, Y., Olshausen, B.A., Gallant, J.L.,
1060 and Rust, N.C. (2005). Do we know what the early visual system does? J. Neurosci. *25*, 10577–
1061 10597.

1062   Castet, E., Lorenceau, J., Shiffrar, M., and Bonnet, C. (1993). Perceived speed of moving lines
1063   depends on orientation, length, speed and luminance. Vision Res. *33*, 1921–1936.

1064   Chavane, F., Sharon, D., Jancke, D., Marre, O., Frégnac, Y., and Grinvald, A. (2011). Lateral
1065   Spread of Orientation Selectivity in V1 is Controlled by Intracortical Cooperativity. Front. Syst.
1066   Neurosci. *5*, 4.

1067   Chemla, S., and Chavane, F. (2010). Voltage-sensitive dye imaging: Technique review and
1068   models. J. Physiol. *104*, 40–50.

1069   Chemla, S., Reynaud, A., di Volo, M., Zerlaut, Y., Perrinet, L., Destexhe, A., and Chavane, F.
1070   (2019). Suppressive traveling waves shape representations of illusory motion in primary visual
1071   cortex of awake primate. J. Neurosci. 2718–2792.

1072   Chen, Y., Geisler, W.S., and Seidemann, E. (2008). Optimal temporal decoding of neural
1073   population responses in a reaction-time visual detection task. J. Neurophysiol. *99*, 1366–1379.

1074   Chen, Y., Palmer, C.R., and Seidemann, E. (2012). The relationship between voltage-sensitive
1075   dye imaging signals and spiking activity of neural populations in primate V1. J. Neurophysiol.
1076   *107*, 3281–3295.

1077   David, S. V., Hayden, B.Y., and Gallant, J.L. (2006). Spectral Receptive Field Properties
1078   Explain Shape Selectivity in Area V4. J. Neurophysiol. *96*, 3492–3505.

1079   DeAngelis, G.C., and Newsome, W.T. (1999). Organization of disparity-selective neurons in
1080   macaque area MT. J Neurosci *19*, 1398–1415.

1081   Desimone, R., Moran, J., Mishkin, M., and Schein, S.J. (1993). A role for the corpus callosum in
1082   visual area V4 of the macaque. Vis. Neurosci.

1083   DiCarlo, J.J., Zoccolan, D., and Rust, N.C. (2012). How does the brain solve visual object
1084   recognition? Neuron *73*, 415–434.

1085   Van Doorn, A.J., and Koenderink, J.J. (1984). Spatiotemporal integration in the detection of
1086   coherent motion. Vision Res. *24*, 47–53.

1087   Engel, A.K., and Fries, P. (2010). Beta-band oscillations--signalling the status quo? Curr. Opin.
1088   Neurobiol. *20*, 156–165.

1089   Van Essen, D.C., and Newsome, W.T. (1984). The visual field representation in the striate cortex
1090   of the macaque monkey: Asymmetries, anisptropies, and indiviual variability. Vision Res. *24*,
1091   429–448.

1092   Florence, S.L., Casagrande, V.A., and Biology, C. (1988). Organization of Individual Cortex in a
1093   Primate Afferent Axons in Layer IV of Striate. *7*.

1094   Fredericksen, R.E., Verstraten, F.A., and van de Grind, W.A. (1994). Spatial summation and its
1095   interaction with the temporal integration mechanism in human motion perception. Vision Res.
1096   *34*, 3171–3188.

1097   Fukushima, K. (1980). Neocognitron: A Self-organizing Neural Network Model for a
1098   Mechanism of Pattern Recognition Unaffected by Shift in Position. Biol. Cybern. *202*, 193–202.

1099   Geisler, W.S. (2008). Visual Perception and the Statistical Properties of Natural Scenes. Annu.
1100   Rev. Psychol. *59*, 167–192.

1101   Georges, S., Seriès, P., Frégnac, Y., and Lorenceau, J. (2002). Orientation dependent modulation

1102   of apparent speed: psychophysical evidence. Vision Res. *42*, 2757–2772.

1103   Girard, P., Hupé, J.M., and Bullier, J. (2001). Feedforward and feedback connections between
1104   areas V1 and V2 of the monkey have similar rapid conduction velocities. J. Neurophysiol. *85*,
1105   1328–1331.

1106   Grinvald, A., and Hildesheim, R. (2004). VSDI: a new era in functional imaging of cortical
1107   dynamics. Nat. Rev. Neurosci. *5*, 874–885.

1108   Grinvald, A., Lieke, E.E., Frostig, R.D., and Hildesheim, R. (1994). Cortical point-spread
1109   function and long-range lateral interactions revealed by real-time optical imaging of macaque
1110   monkey primary visual cortex. J. Neurosci. *14*, 2545–2568.

1111   Gross, C.G., Bender, D.B., and Mishkin, M. (1977). Contributions of the corpus callosum and
1112   the anterior commissure to visual activation of inferior temporal neurons. Brain Res.

1113   Grzywacz, N.M., Watamaniuk, S.N., and McKee, S.P. (1995). Temporal coherence theory for
1114   the detection and measurement of visual motion. Vision Res. *35*.

1115   Guo, K., Nevado, A., Robertson, R.G., Pulgarin, M., Thiele, A., and Young, M.P. (2004). Effects
1116   on orientation perception of manipulating the spatio-temporal prior probability of stimuli. Vision
1117   Res. *44*, 2349–2358.

1118   Guo, K., Robertson, R.G., Pulgarin, M., Nevado, A., Panzeri, S., Thiele, A., and Young, M.P.
1119   (2007). Spatio-temporal prediction and inference by V1 neurons. Eur. J. Neurosci. *26*, 1045–
1120   1054.

1121   Hays, A.V.J., Richmond, B.J., and Optican, L.M. (1982). Unix-based multiple-process system,
1122   for real-time data acquisition and control.

1123   Hubel, D.H., and Wiesel, T.N. (1974). Uniformity of monkey striate cortex: a parallel
1124   relationship between field size, scatter, and magnification factor. J. Comp. Neurol. *158*, 295–305.

1125   Jancke, D., Chavane, F., Naaman, S., and Grinvald, A. (2004a). Imaging cortical correlates of
1126   illusion in early visual cortex. Nature *428*, 423–426.

1127   Jancke, D., Erlhagen, W., Schöner, G., and Dinse, H.R. (2004b). Shorter latencies for motion
1128   trajectories than for flashes in population responses of cat primary visual cortex. J. Physiol. *556*,
1129   971–982.

1130   Judge, S.J., Richmond, B.J., and Chu, F.C. (1980). Implantation of magnetic search coils for
1131   measurement of eye position: An improved method. Vision Res. *20*, 535–538.

1132   Kaplan, B. a., Lansner, A., Masson, G.S., and Perrinet, L.U. (2013). Anisotropic connectivity
1133   implements motion-based prediction in a spiking neural network. Front. Comput. Neurosci. *7*, 1–
1134   14.

1135   Kennedy, H., and Dehay, C. (1988). Functional implications of the anatomical organization of
1136   the callosal projections of visual areas V1 and V2 in the macaque monkey. Behav Brain Res *29*,
1137   225–236.

1138   Kennedy, H., Dehay, C., and Bullier, J. (1986). Organization of the callosal connections of visual
1139   areas V1 and V2 in the macaque monkey. J. Comp. Neurol. *247*, 398–415.

1140   van Kerkoerle, T., Self, M.W., Dagnino, B., Gariel-Mathis, M. -a., Poort, J., van der Togt, C.,
1141   and Roelfsema, P.R. (2014). Alpha and gamma oscillations characterize feedback and
1142   feedforward processing in monkey visual cortex. Proc. Natl. Acad. Sci.

1143 Khoei, M.A., Masson, G.S., and Perrinet, L.U. (2017). The Flash-Lag Effect as a Motion-Based
1144 Predictive Shift. PLoS Comput. Biol. *13*, 1–31.

1145 Klink, P.C., Dagnino, B., Gariel-Mathis, M.A., and Roelfsema, P.R. (2017). Distinct
1146 Feedforward and Feedback Effects of Microstimulation in Visual Cortex Reveal Neural
1147 Mechanisms of Texture Segregation. Neuron *95*, 209-220.e3.

1148 Lenkic, P.J., and Enns, J.T. (2013). Apparent Motion Can Impair and Enhance Target Visibility:
1149 The Role of Shape in Predicting and Postdicting Object Continuity. Front. Psychol.

1150 Liang, H., Gong, X., Chen, M., Yan, Y., Li, W., and Gilbert, C.D. (2017). Interactions between
1151 feedback and lateral connections in the primary visual cortex. Proc. Natl. Acad. Sci. *114*, 8637–
1152 8642.

1153 Liu, J. V., Ashida, H., Smith, A.T., and Wandell, B.A. (2006). Assessment of Stimulus-Induced
1154 Changes in Human V1 Visual Field Maps. J. Neurophysiol.

1155 Lorenceau, J., Shiffrar, M., Wells, N., and Castet, E. (1993). Different motion sensitive units are
1156 involved in recovering the direction of moving lines. Vision Res. *33*, 1207–1217.

1157 MacKay, D.. (1958). Perceptual stability of a stroboscopically lit visual field containing self-
1158 luminous objects. Nature *181*, 507–508.

1159 Marr, D. (1982). Vision: A computational investigation into the human representation and
1160 processing of visual information. (San Francisco).

1161 McKee, S.P., and Welch, L. (1985). Sequential recruitment in the discrimination of velocity. J.
1162 Opt. Soc. Am. A. *2*, 243–251.

1163 Meirovithz, E., Ayzenshtat, I., Bonneh, Y.S., Itzhack, R., Werner-Reiss, U., and Slovin, H.
1164 (2010). Population response to contextual influences in the primary visual cortex. Cereb. Cortex
1165 *20*, 1293–1304.

1166 Movshon, J. a, Adelson, E.H., Gizzi, M.S., and Newsome, W.T. (1985). The analysis of moving
1167 visual patterns. Pattern Recognit. Mech. *54*, 117–151.

1168 Muller, L., Reynaud, A., Chavane, F., and Destexhe, A. (2014). The stimulus-evoked population
1169 response in visual cortex of awake monkey is a propagating wave. Nat. Commun. *5*, 3675.

1170 Muller, L., Chavane, F., Reynolds, J., and Sejnowski, T.J. (2018). Cortical travelling waves:
1171 Mechanisms and computational principles. Nat. Rev. Neurosci.

1172 Mumford, D. (1992). On the computational architecture of the neocortex. Biol. Cybern. *66*, 241–
1173 251.

1174 Nakayama, K., and Silverman, G. (1984). Temporal and spatial characteristics of the upper
1175 displacement limit for motion in random dots. Vision Res.

1176 Nassi, J.J., Lomber, S.G., and Born, R.T. (2013). Corticocortical feedback contributes to
1177 surround suppression in V1 of the alert primate. J. Neurosci. *33*, 8504–8517.

1178 Neri, P. (2014). Dynamic Engagement of Human Motion Detectors across Space-Time
1179 Coordinates. J. Neurosci. *34*, 8449–8461.

1180 Nijhawan, R. (1994). Motion extrapolation in catching. Nature *370*, 256–257.

1181 Orban, G.A., Hoffmann, K.P., and Duysens, J. (1985). Velocity selectivity in the cat visual
1182 system. I. Responses of LGN cells to moving bar stimuli: a comparison with cortical areas 17

and 18. J. Neurophysiol. *54*, 1026–1049.

Pavan, A., Casco, C., Mather, G., Bellacosa, R.M., Cuturi, L.F., and Campana, G. (2011). The effect of spatial orientation on detecting motion trajectories in noise. Vision Res. *51*, 2077–2084.

Perkel, D.J., Bullier, J., and Kennedy, H. (1986). Topography of the afferent connectivity of area 17 in the macaque monkey: a double-labelling study. J. Comp. Neurol. *253*, 374–402.

Perrinet, L.U., and Masson, G.S. (2012). Motion-based prediction is sufficient to solve the aperture problem. Neural Comput. *10*, 24.

Piech, V., Li, W., Reeke, G.N., and Gilbert, C.D. (2013). Network model of top-down influences on local gain and contextual interactions in visual cortex. Proc. Natl. Acad. Sci. *110*, E4108–E4117.

Pigarev, I.N., Nothdurft, H.C., and Kastner, S. (2001). Neurons with large bilateral receptive fields in monkey prelunate gyrus. Exp. Brain Res.

Ramachandran, V.S., and Anstis, S.M. (1983). Extrapolation of motion path in human visual perception. Vision Res. *23*, 83–85.

Ramalingam, N., McManus, J.N.J., Li, W., and Gilbert, C. (2013). Top-down modulation of lateral interactions in visual cortex. J. Neurosci. *33*, 1773–1789.

Rao, R.P., and Ballard, D.H. (1999). Predictive coding in the visual cortex: a functional interpretation of some extra-classical receptive-field effects. Nat. Neurosci. *2*, 79–87.

Reynaud, A., Takerkart, S., Masson, G.S., and Chavane, F. (2011). Linear model decomposition for voltage-sensitive dye imaging signals: application in awake behaving monkey. Neuroimage *54*, 1196–1210.

Reynaud, A., Masson, G.S., and Chavane, F. (2012). Dynamics of local input normalization result from balanced short- and long-range intracortical interactions in area V1. J. Neurosci. *32*, 12558–12569.

Riesenhuber, M., and Poggio, T. (1999). Hierarchical models of object recognition in cortex. Nat. Neurosci. *2*, 1019–1025.

Roach, N.W., McGraw, P. V., and Johnston, A. (2011). Visual motion induces a forward prediction of spatial pattern. Curr. Biol. *21*, 740–745.

Robinson, D.A. (1963). A Method of Measuring Eye Movemnent Using a Scieral Search Coil in a Magnetic Field. Ire Trans. Biomed. Electron. *10*, 137–145.

Roelfsema, P.R. (2006). Cortical Algorithms for Perceptual Grouping. Annu. Rev. Neurosci. *29*, 203–227.

Rust, N.C., Mante, V., Simoncelli, E.P., and Movshon, J.A. (2006). How MT cells analyze the motion of visual patterns. Nat. Neurosci. *9*, 1421–1431.

Schwiedrzik, C.M., Alink, A., Kohler, A., Singer, W., and Muckli, L. (2007). A spatio-temporal interaction on the apparent motion trace. Vision Res. *47*, 3424–3433.

Scott-Brown, K.C., and Heeley, D.W. (2001). The effect of the spatial arrangement of target lines on perceived speed. Vision Res. *41*, 1669–1682.

Shoham, D., Glaser, D.E., Arieli, A., Kenet, T., Wijnbergen, C., Toledo, Y., Hildesheim, R., and Grinvald, A. (1999). Imaging cortical dynamics at high spatial and temporal resolution with

1223   novel blue voltage-sensitive dyes. Neuron *24*, 791–802.

1224   Simoncelli, E.P., and Heeger, D.J. (1998). A model of neuronal responses in visual area MT.
1225   Vis. {R}esearch *38*, 743–761.

1226   Slovin, H., Arieli, A., Hildesheim, R., and Grinvald, A. (2002). Long-term voltage-sensitive dye
1227   imaging reveals cortical dynamics in behaving monkeys. J. Neurophysiol. *88*, 3421–3438.

1228   Snowden, R., and Braddick, O. (1989a). Extension of displacement limits in multiple-exposure
1229   sequences of apparent motion. Vision Res. *29*, 1777–1787.

1230   Snowden, R.J., and Braddick, O.J. (1989b). The combination of motion signals over time. Vision
1231   Res. *29*, 1621–1630.

1232   Srinivasan, M. V, Laughlin, S.B., and Dubs, A. (1982). Predictive coding: a fresh view of
1233   inhibition in the retina. Proc. R. Soc. Lond. B. Biol. Sci. *216*, 427–459.

1234   Stettler, D.D., Das, A., Bennett, J., and Gilbert, C. (2002). Lateral connectivity and contextual
1235   interactions in macaque primary visual cortex. Neuron *36*, 739–750.

1236   Subramaniyan, M., Ecker, A.S., Patel, S.S., Cotton, R.J., Bethge, M., Pitkow, X., Berens, P., and
1237   Tolias, A.S. (2018). Faster processing of moving compared with flashed bars in awake macaque
1238   V1 provides a neural correlate of the flash lag illusion. J. Neurophysiol. *120*, 2430–2452.

1239   Sundberg, K.A., Fallah, M., and Reynolds, J.H. (2006). A motion-dependent distortion of
1240   retinotopy in area V4. Neuron *49*, 447–457.

1241   Swindale, N. V (1998). Biological Cybernetics Orientation tuning curves : empirical description
1242   and estimation of parameters. *56*, 45–56.

1243   Takerkart, S., Fenouil, R., Piovano, J., Reynaud, A., Hoffart, L., Chavane, F., Papadopoulo, T.,
1244   Conrath, J., and Masson, G.S. (2008). A quantification framework for post-lesion neo-
1245   vascularization in retinal angiography. In 2008 5th IEEE International Symposium on
1246   Biomedical Imaging: From Nano to Macro, Proceedings, ISBI, pp. 1457–1460.

1247   Tlapale, E., Masson, G.S., and Kornprobst, P. (2010). Modelling the dynamics of motion
1248   integration with a new luminance-gated diffusion mechanism. Vision Res. *50*, 1676–1692.

1249   Tootell, R.B.H., Silverman, M.S., Switkes, E., and De Valois, R.L. (1982). Deoxyglucose
1250   analysis of retinotopic organization in primate striate cortex. Science (80-.).

1251   Ullman, S. (1979). The interpretation of structure from motion. Proc. R. Soc. Lond. B. Biol. Sci.
1252   *203*, 405–426.

1253   Verghese, P., and Watamaniuk, S. (1999). Local motion detectors cannot account for the
1254   detectability of an extended trajectory in noise. Vision Res. *39*, 19–30.

1255   Verghese, P., McKee, S.P., and Grzywacz, N.M. (2000). Stimulus configuration determines the
1256   detectability of motion signals in noise. J. Opt. Soc. Am. A. Opt. Image Sci. Vis. *17*, 1525–1534.

1257   W. Metzger (1932). No TitleVersuch einer gemeinsamen Theorie der Phänomene Fröhlichs und
1258   Hazelhoffs und Kritik ihrer Verfahren zur Messung der Empfindungszeit. Psychol. Forsch. *16*,
1259   176–200.

1260   Wallach, H. (1935). Über visuell wahrgenommene Bewegungsrichtung. Psychol. Forsch. *20*,
1261   325–380.

1262   Watamaniuk, S.N., and McKee, S.P. (1995). Seeing motion behind occluders. Nature *377*, 729–

1263   730.

1264   Watamaniuk, S.N., McKee, S.P., and Grzywacz, N.M. (1995). Detecting a trajectory embedded
1265   in random-direction motion noise. Vision Res. *35*, 65–77.

1266   Watanabe, J., and Nishida, S. (2007). Veridical perception of moving colors by trajectory
1267   integration of input signals. J. Vis. *7*, 3.1-16.

1268   Welch, L., Macleod, D.I., and Mckee, S.P. (1997). Motion interference: perturbing perceived
1269   direction. Vision Res. *37*, 2725–2736.

1270   Werkhoven, P., Snippe, H.P., and Koenderink, J.J. (1990). Effects of element orientation. *47*,
1271   509–525.

1272   Wertheimer, M. (1912). Experimentelle studien über das sehen von bewegung. Z. Psychol. *61*.

1273   Wilson, H.R., Ferrera, V.P., and Yo, C. (1992). A psychophysically motivated model for two-
1274   dimensional motion perception. Vis. Neurosci. *9*, 79–97.

1275   Yuille, A.L., and Grzywacz, N.M. (1989). A mathematical analysis of the motion coherence
1276   theory. Int. J. Comput. Vis. *3*, 155–175.

1277

1278   **SUPPLEMENTARY MATERIAL**

1279

1280   **Figure supplement 1.**

1281
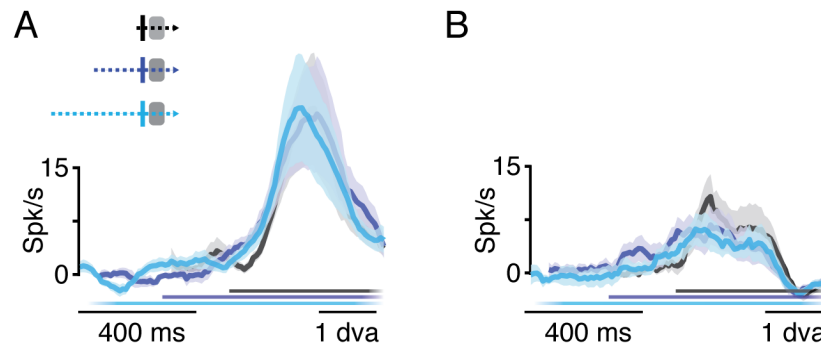
1282   **Suppl. Figure 1: Average PSTHs across non-anticipatory neurons for the three trajectories**.
1283   (**A**) Average PSTHs across non-anticipatory neurons for the three trajectories for monkey PD (n=20).
1284   Responses are aligned to the latency of the short trajectory condition. Color lines (bottom) indicate the
1285   stimulus presentation time, for each condition. No significant difference with respect to the short
1286   trajectory condition were detected (Two-sample t-test P>0.05). (**B**) Same than A but for monkey NO
1287   (n=3).

1288

1289

1290

Figure supplement 2: Anticipation is not caused by eye movements or excessively large RF

In order to completely exclude potential effects of eye movements or changes in receptive field size to the observed anticipation, we conducted several control experiments. First, we computed the distribution of eye positions across all successful trials of the 3-trajectories paradigm for 22 cells (a smaller number of cells is used here because the eye-movements recorded in some experimental sessions were deteriorated due to an error in the data acquisition software). Our results show that 99% of eye positions were distributed within 1dva around the fixation spot and with identical distribution for the 3 conditions (**Supp. Figure 2A**). Thus, any changes in RF location due to eye movements would have been much smaller than the 2.3 (PD) and 3 dva (NO) equivalent distance reported for the average anticipatory responses in the two monkeys.

Second, comparing the skewness of the distributions in Figure 1A for long (y-axis) and short trajectory conditions (x-axis), we showed that there is not difference in the slant towards of (negative values) or away from (positive values) the direction of the approaching bar (**Supp. Figure 2B**).

Third, we recomputed mean response profiles as a function of the actual distance of the bar from the RF center when considering the real-time position of eye fixation (acquisition rate 2Hz) (**Supp. Figure 2C**). This analysis (A-C) was applied to the 22 cells for which we had high quality eye-movements recordings. The anticipatory responses for medium (3dva) and long (6dva) trajectories were still significant in all the anticipatory cells tested (n=7), rejecting the possibility that they could be a mere consequence of a systematic bias or transient events in fixation behavior. On the contrary, the overall response across the 22 cells tested presents an increase in the anticipatory response after correcting for the real-time position of the eye.

Fourth, we confirmed that anticipatory responses are not simply explained by a sampling bias for large receptive fields (**Supp. Figure 2D, E, F**). The anticipation is plotted in spatial coordinate as a function of the receptive field radius for medium (1D) and long (1E) trajectories. The anticipation started systematically outside of the classical RF (above the main diagonal) and most of the points are also further away than twice the size of the classical RF (above y=2x). We also compared the p-value of the statistical test for the significance of the anticipatory response (relative to baseline) and showed that there is not trends, actually the smallest p-values are observed for the smallest RF.
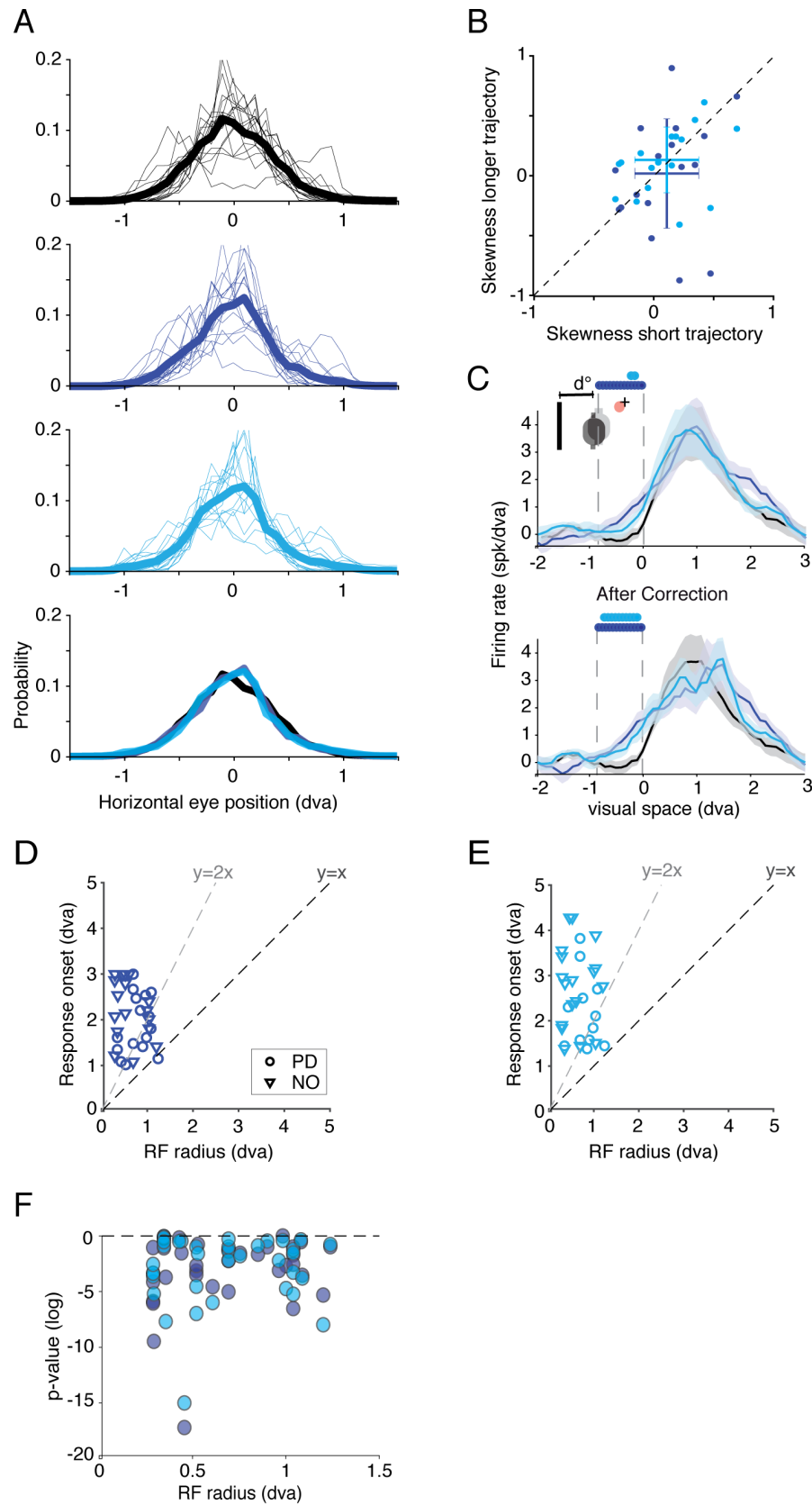
Suppl. Figure 2: Test existence of biases from eye movements and RF sizes in the emergence of anticipatory responses. (**A**) Gaze positions distribution across all successful trials for all 3-trajectories conditions (black), thin traces are single cells, thick trace the average, which are plotted for the 3 conditions in the same graph in the bottom (n = 22 cells). (**B**) for all cells we measured the skewness of the distribution in A to test whether a slant towards (negative) or away (positive values) of the direction of the approaching bar was existing for long trajectories (y-axis) compared to the short trajectory condition (x-axis). The average and std across cells is presented as error bars. (**C**) Eye movement correction control. Average PSTHs among cells (n=22 cells) for the three conditions before and after eye movement correction of the spikes timing relative to the exact distance between the receptive field and the bar. Neural response is therefore expressed in number of spikes per degree of visual angle of the bar displacement (spk/dva), assuming a constant latency of 50ms. Upper left inset sketch the RF position correction (grey before, dark after correction) due to eye position (red dot) relative to the central fixation ('+'), allow to compute the exact distance (d in dva) between the bar and the RF. Colored lines (top) indicate significant difference with respect to the short trajectory condition (two-sample t-test P<0.05) before the bar enters the RF (i.e. 0 dva). (**D-E**) Position of the bar at response onset (y-axis) as a function of RF size for the medium and long-trajectory conditions. The main diagonal (y=x) and twice the main diagonal (y=2x) are shown to compare the position of the bar that evoked anticipatory activity with extreme limits of RF when mapped using classical procedures. (**F**) p-value of the anticipatory activity t-test (relative to spontaneous activity) as a function of its RF size (n = 36).

1361   **Figure supplement 3.**
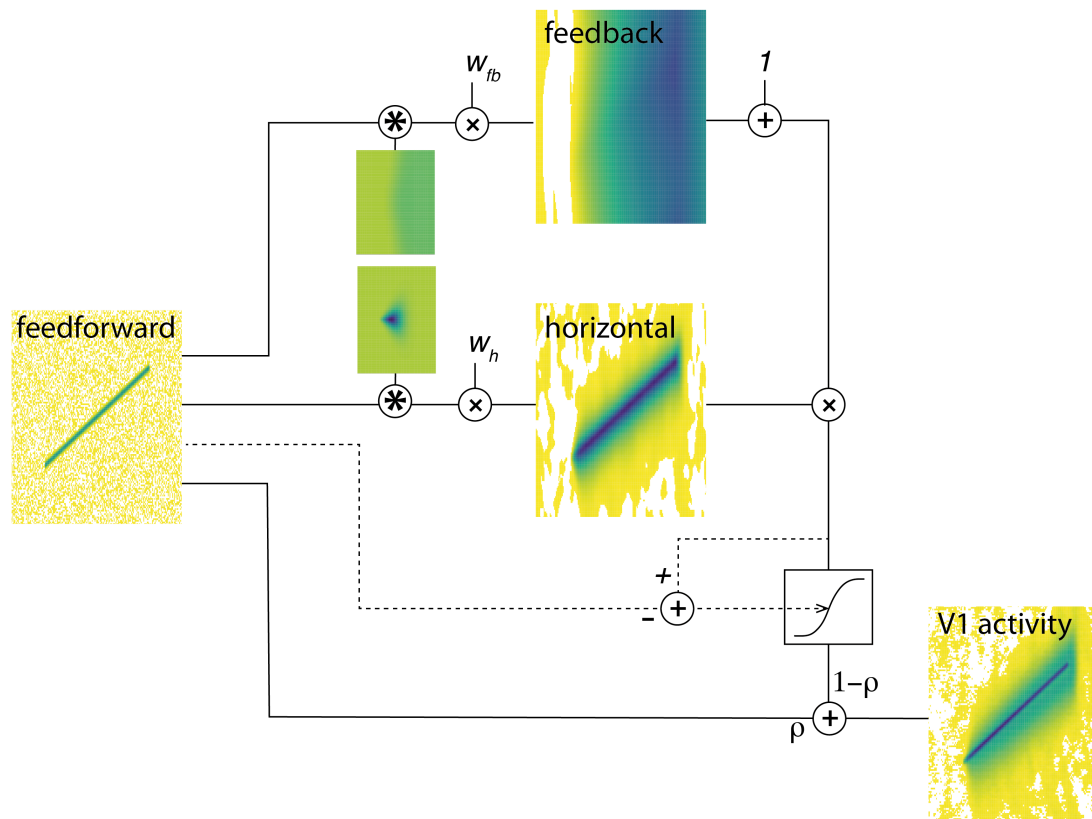
1362

1363   **Suppl. Fig 3: Block diagram sketch of the computational model.** From left to right is depicted
1364   the logical flow of our model. The matrices of the diagram all represents space in y and time in
1365   x. On the left is represented the feedforward predicted activation of V1 to a bar moving at
1366   6.6dva/s other an extended trajectory. At that level, random noise is added to the simulated
1367   activation. To generate horizontal or feedback activation maps, the feedforward matrix is
1368   convolved with kernels with low extent low speed (horizontal) and large extent fast speed
1369   (feedback), and then weighted by w_h and w_{fb}. The feedback activation map is then added a scalar
1370   of 1 and multiplied to the horizontal activation map to amplify of the horizontal activation
1371   (Liang et al., 2017; Ramalingam et al., 2013, Piech et al 2013). The resulting activation map is
1372   then passing through a sigmoid non-linearity controlled by the difference between the
1373   feedforward and the horizontal-feedback activation maps. The relative contribution of the
1374   feedforward and horizontal-feedback maps are then summed with a ratio of ρ, to generate the
1375   predicted V1 activity.